TECHNOLOGICAL UNIVERSITY DELFT

DEPARTMENT OF AERONAUTICAL ENGINEERING

Report VTH-124

THEORETICAL AND EXPERIMENTAL INVESTIGATIONS OF INCOMPRESSIBLE LAMINAR BOUNDARY LAYERS WITH AND WITHOUT SUCTION

Ph.D THESIS

J.L. van INGEN

DELFT
the NETHERLANDS

OCTOBER, 1965

This PDF-file contains chapter 8:

Some applications of the new calculation methods

8. Some applications of the new calculation methods.

8.1. Introductory remarks.

The present chapter contains some applications of the new calculation methods discussed in chapters 5 and 7. The results will be compared to available exact solutions. If for a specific example no results of the momentum method are quoted they have been presented already in chapter 5.

8.2. The flat plate without suction.

For the flat plate without suction $\frac{d\bar{U}}{d\bar{x}} = v_o = 0$ and hence equations (7.58) and (7.59) show that $\lambda_1 = \lambda_2 = 0$. Equations (7.62) and (7.63) then lead to $a_1 = a_2 = 0$ while from (7.61) it follows that $a_3 = -1/6$ if a similar solution with $\frac{da_o}{d\bar{x}} = 0$ is to be obtained.
The values of a_o, a_4, a_5, ... are determined by equations (7.64) to (7.66). It is noted that the equations are non-linear and therefore may possess several solutions. For instance, a solution of the complete set of equations (7.61) to (7.66) is $a_n \equiv 0$ for all values of N which however is physically unrealistic. For N = 4 no moment equations are needed and the remaining equations (7.61) to (7.65) have only one solution in addition to the irrelevant one $a_n = 0$. The solution is found to be $a_o = 1/24 = 0.041667$; $a_1 = a_2 = 0$; $a_3 = -1/6$ and $a_4 = 1/8$. From Blasius' theory, discussed in section 3.1.3, it is known that $a_o = \frac{\tau_o x}{\mu U}\sqrt{\frac{\nu}{Ux}} = 0.33206$ or $a_o = 0.11026$ which shows that the approximation to the exact solution is rather poor for N = 4. A substantial improvement is obtained however for $N > 4$, which implies the use of moment equations. Results for N = 5 to 9 were obtained, using the procedures outlined in section 7.8; as starting value for a_o in the iteration method $a_o = 0.11$ was used throughout. Since the final results for the a_n show a regular pattern (see table 8.1) it was easy to estimate good starting values for the other a_n's at $N = N_1$ once the results for $N < N_1$ were known.
It may be remarked that no difficulties were encountered from the occurrence of multiple solutions; in a wide region around the relevant one there were no other solutions.

Values for the a_n's at different values of N have been collected in table 8.1. From the formulae given in section 7.10 the functions $S(\bar{u})$, the velocity profiles and some familiar boundary layer parameters were calculated. The results are given in table 8.2 and figs 8.1 and 8.3. All data show a monotonic convergence towards the exact solution with increasing values of N. However, the convergence slows down for $N > 7$ and therefore it seems to be of little use to go beyond N = 7 or 8 for practical applications. Table 8.2. and fig. 8.3. show, that in this way the usual boundary layer parameters are predicted within a few percent of the exact values.

The results, given in table 8.2, suggest that the differences with the exact solution are approximately halved if N is increased from 6 to 7 or from 7 to 8. Hence to obtain a more accurate result from the values for N = 6 and 7 corrected values for N = 7 - to be denoted by $N = 7^*$ - may be determined from

$$a_n^* = 2(a_n)_{N=7} - (a_n)_{N=6} \qquad (8.1)$$

The corrected results, obtained in this way, have been included in tables 8.1 and 8.2. The $S(\bar{u})$ and velocity profiles for $N = 7^*$ are found to be so close to the exact solution that they have not been shown in fig. 8.1.

8.3. The plane stagnation point without suction.

For the plane stagnation point the potential flow velocity distribution is given by $\bar{U} = u_1\bar{x}$ (equation 3.19). Hence it follows that $\lambda_1 = 1$ and since $v_o = 0$ the suction parameter λ_2 is equal to zero.

Results for different values of N have been determined in the same way as described in section 8.2 for the flat plate. The final results have been collected in tables 8.3 and 8.4 and figs 8.2 and 8.3.

It follows that the approximation to the exact solution is better than for the flat plate. Again more accurate results can be obtained from the results for N = 6 and 7 using equation (8.1). The results for $N = 7^*$, 8, 9 and 10 are so close to the exact values that they could not be shown in fig. 8.2.

8.4. Hartree's boundary layers without suction.

For the Hartree boundary layers the pressure distribution is defined by $\bar{U} = u_1 \bar{x}^{m_1}$ (see equation 3.1 and section 3.1.2.). Hence it follows that $\lambda_1 = m_1$ and equation (3.4) then gives

$$\lambda_1 = \frac{\beta}{2-\beta} \qquad (8.2)$$

For several values of β between $\beta = 1$ (plane stagnation point) and $\beta = -0.198838$ (separation according to the exact solution) calculations have been made in the same way as described in sections 8.2 and 8.3 for the special cases $\beta = 0$ and $\beta = 1$. Results for a_o, which is essentially the square of the wall shear stress, are shown in figs 8.5a and 8.5b. It follows that a_o converges monotonically towards the exact solution for $\beta > -0.06$. Near separation however, ($\beta < -0.06$) a_o first decreases when N is increased from 5 to 6 and then increases towards the exact solution. Detailed results for $\beta = -0.16$ are given in table 8.5 while the velocity profiles are shown in fig. 8.6. It follows that not only a_o but also other relevant parameters show a non-monotonic convergence to the exact solution.

Figs 8.7 and 8.8 show the exact values of $S = \bar{\tau}^{-2}$ and $\bar{\tau}$ as function of $\bar{u}$ for a series of values for β.

From fig. 8.8 it is seen that $\bar{\tau}$ behaves like $\sqrt{\bar{u}}$ near the wall ($\bar{u} = 0$) for the separation profile. This illustrates the advantage of using $\bar{\tau}^{-2}$ instead of $\bar{\tau}$ as dependent variable.

8.5. The flat plate with $v_o \backsim x^{-\frac{1}{2}}$.

For this similar solution (see section 5.4.4) $\lambda_1 = 0$ and $\lambda_2 = \frac{-v_o}{U}\sqrt{\frac{Ux}{\nu}}$ is an arbitrary constant.

Both from the exact solution and from the momentum method (see section 5.4.4) it is known that for this flow the boundary layer tends to the asymptotic suction layer for $\lambda_2 \to \infty$. This result also holds for the multimoment method. For $\lambda_2 = 0$ of course the flat plate without suction, discussed in section 8.2, is obtained.

For other values of λ_2 calculations were performed for different values

of N; the parameter a_o for N = 5 is shown in fig. 8.4 and compared to the exact results due to Thwaites [66] and Schlichting-Bussmann (quoted by Mangler [37]). Only the results for N = 5 are shown in the figure since those for higher values of N are close to the exact solution.

8.6. The plane stagnation point with constant suction velocity.

For the plane stagnation point $\lambda_1 = 1$ (see section 8.3) and to obtain a similar solution $\lambda_2 = \frac{-v_o}{U}\sqrt{\frac{Ux}{\nu}}$ should be constant. For $\lambda_2 = 0$ the plane stagnation point without suction is obtained while for $\lambda_2 \to \infty$ the asymptotic suction layer is found.
Results of the multimoment method for N = 5 are shown in fig. 8.9 and compared to the exact solution of Schlichting-Bussmann (quoted by Mangler [37]).

8.7. Howarth' boundary layer flow for $\bar{U} = 1 - \bar{x}$ without suction.

8.7.1. General.

In [44] Howarth studied the boundary layer flow corresponding to a main stream velocity U defined by

$$U = b_o - b_1 x \tag{8.4}$$

in which b_o and b_1 are constants. Defining the reference speed U_∞ and -length c by

$$U_\infty = b_o \quad \text{and} \quad c = \frac{b_o}{b_1} \tag{8.5}$$

equation (8.4) reduces to

$$\bar{U} = 1 - \bar{x} \tag{8.6}$$

This boundary layer was calculated by Howarth using a series method with the following expansion for the stream function

$$\psi = \sqrt{2\, U_\infty \nu\, x}\left[f_o(\eta) + \bar{x}\, f(\eta) + \bar{x}^2 f_2(\eta) + \ldots \right] \tag{8.7}$$

in which

$$\eta = \sqrt{\frac{U_\infty}{2\nu x}}\, y \qquad (8.8)$$

(see also section 3.2.3.).

The function $f_o(\eta)$ was shown to satisfy the Blasius equation (3.14) while the functions $f_n(\eta)$ for $n > 1$ had to be calculated from a set of linear differential equations. Howarth calculated the functions f_n for $n \leq 6$ which however was not sufficient for an accurate determination of the separation point. Therefore the result was improved as follows. It was noted by Howarth that the functions $f_5(\eta)$ and $f_6(\eta)$ have the same shape and this led him to assume that all f_n for $n \geq 5$ are the same in shape so that equation (8.7) can be written in the form

$$\psi = \sqrt{2U_\infty \nu x}\left[\sum_0^6 \bar{x}^n f_n(\eta) + A(\bar{x})\, f_6(\eta)\right] \qquad (8.9)$$

The function $A(\bar{x})$ is different from zero only in regions where the series (8.7) is not sufficiently convergent using 7 terms only; this occurs near separation. The function $A(\bar{x})$ was determined by Howarth from the requirement that (8.9) should satisfy the von Kármán momentum equation (2.15). In this way separation was found at $\bar{x} = 0.120$; this result was confirmed from later calculations made by Hartree [81], Tani [45], Leigh [82] and Terrill [83].

8.7.2. The momentum method.

For $\bar{U} = 1 - \bar{x}$ the momentum equation (5.18) can be written in the form

$$\frac{d\bar{\theta}^2}{d\bar{x}} = \frac{M}{1-\bar{x}} \qquad (8.10)$$

which can be integrated to

$$-\ln(1-\bar{x}) = \int_0^{\bar{\theta}^2} \frac{d\bar{\theta}^2}{M} \qquad (8.11)$$

From $\bar{U} = 1 - \bar{x}$ it follows that in this case the pressure gradient

parameter $\Lambda_1 = \bar{\theta}^2 \frac{d\bar{U}}{d\bar{x}}$ reduces to $\Lambda_1 = -\bar{\theta}^2$. Since in the no-suction case M is a function of Λ_1 only (see table 5.3 and fig. 5.6) this parameter can also be considered as a function of $\bar{\theta}^2$. Hence the integral (8.11) can easily be calculated. Some results are shown in fig. 8.10 and compared to the exact solution due to Howarth. Separation is found at $\bar{x} = 0.123$ as compared with $\bar{x}_{sep} = 0.120$ for the exact solution. A comparison of the velocity profiles for $\bar{x} = 0.10$ and 0.12 is shown in fig. 8.11.

8.7.3. The multi-moment method.

For $\bar{U} = 1 - \bar{x}$ the pressure gradient parameter λ_1 becomes

$$\lambda_1 = \frac{\bar{x}}{\bar{U}} \frac{d\bar{U}}{d\bar{x}} = \frac{-\bar{x}}{1-\bar{x}} \tag{8.12}$$

and hence the power series expansion (7.80) for λ_1 is easily found to be

$$\lambda_1 = -\bar{x} - \bar{x}^2 - \bar{x}^3 - \bar{x}^4 \ldots\ldots \tag{8.13}$$

Since the zero-order term in (8.13) is absent it follows that the boundary layer at $\bar{x} = 0$ will start as the similar solution for which $\lambda_1 = 0$; this is the flat plate boundary layer, discussed in section 8.2. Therefore the zero-order terms of the expansion for a_n follow from table 8.1.

Results for a_o at N = 7 and different orders p of the series solution are shown in fig. 8.12. It follows that the series converges well until very close to separation. Included in the figure as a dotted line is the result of a step by step calculation started at $\bar{x} = 0.08$.

Fig. 8.12 shows that in the step by step solution zero skin friction is only asymptotically reached. This behaviour is caused by equation (7.61) which for zero suction ($a_2 = \lambda_2 = 0$) reduces to

$$\frac{da_o}{d\bar{x}} \longrightarrow 0 \qquad \text{for} \qquad a_o \longrightarrow 0 \tag{8.14}$$

This anomalous behaviour is the prize to be paid for the convenience of using equation (7.61) which gives an easy means to determine a_o. In section 8.14 this difficulty will be discussed further.
Results for different values of N have been collected in fig. 8.13; in each case the series method was used from $\bar{\bar{x}} = 0$ to 0.08 including terms of the 10th degree in $\bar{x}$. Downstream of $\bar{x} = 0.08$ the step by step method was used; for all values of N differences between the series- and step by step solutions became noticeable only for $\bar{x} > 0.10$. Included in fig. 8.13 are the values of a_o according to the exact solution.
It should be noted that far from separation there is a monotonic convergence to the exact solution with increasing N. Near separation however, the convergence is of the type displayed by the Hartree flows for $\beta < -0.06$.
A comparison of figs 8.10 and 8.13 shows that the momentum method and the multimoment method with N = 8 have about the same accuracy for a_o. Results of Görtler's series for $\sqrt{a_o}$ and a_o are given in fig. 8.14 and 8.15. It follows that Görtler's method, which is exact at $\bar{x} = 0$, is not very accurate near separation due to lack of convergence. The present series method is in this region at least equally accurate and moreover easily allows a step by step continuation.
Finally fig. 8.16 shows, to a large scale, results for a_o in the region near separation according to different methods.

8.8. Tani's boundary layers for $\bar{U} = 1 - \bar{x}^j$.

Using essentially Howarth' procedure (see section 8.7.1) the boundary layer flows for

$$\bar{U} = 1 - \bar{x}^j \tag{8.15}$$

have been calculated by Tani [45] for j = 2, 4 and 8. The position of the separation point obtained in this way is shown in table 8.6.

For $\bar{U} = 1 - \bar{x}^j$ without suction $\lambda_2 = 0$ while λ_1 becomes

$$\lambda_1 = \frac{\bar{x}}{\bar{U}} \frac{d\bar{U}}{d\bar{x}} = - \sum_{i=1}^{\infty} j\left(\bar{x}^j\right)^i \tag{8.16}$$

Introducing a new variable z according to equation (7.79) with f = j, equation (8.16) may be written in the form

$$\lambda_1 = - \sum_{p=1}^{\infty} j\, z^p \tag{8.17}$$

Since (8.16) and (8.17) do not contain a zero-order term it follows that the multimoment method reproduces the result from exact theory that Tani's boundary layers start at $\bar{x} = 0$ in the same way as the Blasius boundary layer.

Detailed results of the multimoment method with N = 7 for $\bar{U} = 1 - \bar{x}^2$ are shown in fig. 8.17. It follows that the series solution including terms with $\bar{x}^{20}$ gives a good correspondence with the step by step solution until close to separation.

Final results for N = 5, 6 and 7 are shown in fig. 8.18 where also a comparison is made with the exact solution due to Tani. It is seen that an accurate extimate of the position of separation can be obtained from a linear extrapolation of a_o for $\bar{x} < 0.26$.

In the same way results have been obtained for j = 4 and 8. The positions of separation for j = 1, 2, 4 and 8 at N = 7 are collected in table 8.6.

8.9. The boundary layer on a circular cylinder without suction: $\bar{U} = \sin \bar{x}$.

8.9.1. General.

Boundary layer calculations for the pressure distribution corresponding to potential flow around a circular cylinder have been made by many authors. Possibly the most accurate result has been obtained to date by Terrill [83], using a numerical procedure.

For this flow the velocity U is given by (see fig. 8.19)

$$U = 2V \sin \varphi = 2V \sin\left(\frac{x}{R}\right) \tag{8.18}$$

If the reference speed and -length U_∞ and c are defined by

$$U_\infty = 2V \quad ; \quad c = R \tag{8.19}$$

equation (8.18) reduces to

$$\bar{U} = \sin \bar{x} \tag{8.20}$$

8.9.2. The momentum method.

For small $\bar{x}$ equation (8.20) reduces to $\bar{U} = \bar{x}$ which shows that the boundary layer on the circular cylinder starts near $\bar{x} = 0$ as the plane stagnation point flow. Hence starting values for the step by step calculation can be obtained from section 5.4.2. Results for a_o are shown in fig. 8.20 and compared to the exact solution due to Terrill. The momentum method gives separation at $\bar{x} = 1.78$ while the accurate value is 1.823.

8.9.3. The multimoment method.

With $\bar{U} = \sin \bar{x}$ the expression for λ_1 becomes

$$\lambda_1 = \frac{\bar{x}}{\bar{U}} \frac{d\bar{U}}{d\bar{x}} = \bar{x} \frac{\cos \bar{x}}{\sin \bar{x}} \tag{8.21}$$

which can be developed in the following power series

$$\lambda_1 = 1 - \frac{1}{3}\bar{x}^{-2} - \frac{1}{45}\bar{x}^{-4} - \frac{2}{945}\bar{x}^{-6} - \frac{1}{4725}\bar{x}^{-8} - \frac{2}{93555}\bar{x}^{-10} \ldots\ldots \tag{8.22}$$

Since in (8.22) the zero order term is 1 the boundary layer starts at $\bar{x} = 0$ in the same way as the plane stagnation point without suction discussed in section 8.3. Hence, the zero-order terms of the series for a_n can be obtained from table 8.3. Results of the series method up till and including terms with $\bar{x}^{-10}$ have been obtained for N = 5, 6 and 7. The series (8.22) contains only terms of even order and hence this is also the case with the resulting series for a_n. Results for a_o at N = 7 and different orders of the approximation are shown in fig. 8.20; the

curve for p = 8 which is not shown lies between those for p = 6 and 10. Results of a step by step calculation started at $\bar{x} = 1.50$ are shown as a dotted line in fig. 8.20. It follows from the figure that only near separation the step by step solution differs from the series solution for p = 10. It should be emphasized that - in principle - the present series method can be used to much higher orders p which certainly would improve the correspondence between the step by step- and the series solution. However, this has not been done in the present example since it is very easy to continue with the step by step calculation.

Results for N = 5 and 6 are very close to those for N = 7 and therefore have not been given in fig. 8.20. Only near separation the solutions for N = 5 and 6 lay slightly above those for N = 7.

Included in fig. 8.20 are the exact results due to Terrill; for this solution separation occurs at $\bar{x} = 1.823$. It is seen that the multimoment method for N = 7 accurately approximates the exact solution except very near separation. However, with a short linear extrapolation of a_o for $\bar{x} < 1.80$ an accurate estimate of the separation point is obtained.

Results obtained from Görtler's series are shown in fig. 8.21 and 8.22; the figure for $\sqrt{a_o}$ is included since Görtler's method employs variables which express the wall shear stress in a parameter equivalent to $\sqrt{a_o}$ instead of a_o.

A comparison of figs 8.21 and 8 22 clearly shows the advantage of using $\bar{\tau}^2$ instead of $\bar{\tau}$ (and hence a_o instead of $\sqrt{a_o}$) as dependent variable.

Near a separation point $\bar{x}_{sep}$, the function a_o behaves like

$$a_o \lesssim (\bar{x} - \bar{x}_{sep})^1 \tag{8.23}$$

and hence

$$\sqrt{a_o} \lesssim (\bar{x} - \bar{x}_{sep})^{\frac{1}{2}} \tag{8.24}$$

(see also Goldstein [84] and Terrill [83]).

Of course it is easier to approximate (8.23) with a series than (8.24).

From a comparison of figs 8.20 and 8.21 it follows that both the momentum method and the multimoment method give a better accuracy near separation than Görtler's method.

8.10. Curle's boundary layer flow for $\bar{U} = \bar{x} - \bar{x}^3$.

8.10.1. General.

The boundary layer flow for the pressure distribution defined by

$$\bar{U} = \bar{x} - \bar{x}^3 \tag{8.25}$$

has been calculated by Curle [85] using Howarth' procedure, described in section 8.7.1. For this boundary layer separation was found at $\bar{x} = 0.655$.

8.10.2. The momentum method.

For small values of $\bar{x}$ equation (8.25) reduces to $\bar{U} = \bar{x}$ and hence the boundary layer starts as the plane stagnation point. Hence the step by step calculation can be started at a small distance from the stagnation point ($\bar{x} = 0$) with a starting value for $\bar{\theta}$ obtained from section 5.4. Results for a_o are shown in fig. 8.23 and compared to the exact solution; separation is predicted at $\bar{x} = 0.640$.

8.10.3. The multi-moment method.

With $\bar{U} = \bar{x} - \bar{x}^3$ the series expansion for λ_1 becomes

$$\lambda_1 = 1 - 2\,\bar{x}^2 - 2\,\bar{x}^4 - 2\,\bar{x}^6 \ldots . \tag{8.26}$$

which again shows that the boundary layer starts at $\bar{x} = 0$ as the plane stagnation point. Calculations have been performed for N = 5, 6 and 7 using the series method from $\bar{x} = 0$ to 0.55 and the step by step method downstream of $\bar{x} = 0.55$. Final results for N = 7 are shown in fig. 8.23 where also the exact solution is shown. Results for N = 5 and 6 are so close to those for N = 7 that the differences cannot be shown in the figure except very close to separation. Only the results for N = 5 are shown, those for N = 6 are between those for N = 5 and 7. It follows that the multimoment method gives a very good approximation to the exact solution. Also near separation the accuracy is gradually improved with increasing N. Although for this example again separation is reached with

$\frac{da_o}{d\bar{x}} \rightarrow 0$ the curve for a_o bends so sharply into the horizontal axis, especially for N = 7, that a short linear extrapolation is sufficient to provide an accurate determination of the separation point. From a large scale version of fig. 8.23 the value of $\bar{x}$ at separation was found to be $\bar{x} = 0.652$ which is very close to the exact value 0.655.

8.11. Iglisch' solution for the flat plate with constant suction velocity.

8.11.1. General.

For the flat plate with constant suction velocity v_o, an exact solution of the boundary layer equations has been given by Iglisch [67]. In this solution a new independent variable $\bar{x}$ is introduced by

$$\bar{x} = \frac{x}{c} = \left(\frac{-v_o}{U}\right)^2 \frac{Ux}{\nu} \tag{8.27}$$

which implies that the reference length c is defined by

$$c = \frac{U\nu}{(-v_o)^2} \tag{8.28}$$

If for the reference speed U_∞ the constant main stream velocity U is used it follows that

$$\bar{U} = \frac{U}{U_\infty} = 1 \tag{8.29}$$

From Iglisch' solution it is known that at $\bar{x} = 0$ the boundary layer starts as the Blasius boundary layer while for $\bar{x} \rightarrow \infty$ the asymptotic suction layer is obtained.

8.11.2. The momentum method.

Using equations (8.27) to (8.29) it follows that for the present case

$$\bar{v}_o = \frac{-v_o}{U_\infty}\sqrt{\frac{U_\infty c}{\nu}} = 1 \tag{8.30}$$

$$\Lambda_1 = \bar{\theta}^2 \frac{d\bar{U}}{d\bar{x}} = 0 \tag{8.31}$$

and $$\Lambda_2 = \bar{v}_o\,\bar{\theta} = \bar{\theta} \tag{8.32}$$

Hence the momentum equation (5.18) reduces to the simple form

$$\frac{d(\Lambda_2^2)}{d\bar{x}} = \ell - \Lambda_2 \tag{8.33}$$

which can be written as

$$\bar{x} = \int_0^{\Lambda_2} \frac{\Lambda_2}{\ell - \Lambda_2}\, d\Lambda_2 \tag{8.34}$$

Since for the flat plate $\Lambda_1 = 0$, the parameter ℓ is a known function of Λ_2 (see chapter 5) and equation (8.34) can easily be integrated numerically. It follows from equation (8.34) that $\bar{x} \to \infty$ for $\ell \to \Lambda_2$; this occurs for $\ell = \Lambda_2 = 0.50$ which represents the asymptotic suction profile. Since the momentum method was designed to represent the asymptotic suction layer exactly it follows that the method gives exact results for $\bar{x} \to \infty$.

For $\bar{x} = 0$ the momentum loss thickness θ is zero and hence $\Lambda_2 = \frac{-v_o \theta}{\nu} = 0$; which implies that the boundary layer starts at $\bar{x} = 0$ as that on a flat plate without suction.

Different parameters are shown as a function of $\sqrt{\bar{x}}$ in fig. 8.24 and compared to Iglisch' exact solution and an approximate solution due to Schlichting [55] (see also section 4.3).

.11.3. The multimoment method.

From equations (8.27) and (8.29) it follows that

$$\lambda_1 = \frac{\bar{x}}{\bar{U}}\,\frac{d\bar{U}}{d\bar{x}} = 0 \tag{8.35}$$

and $$\lambda_2 = \frac{-v_o}{U}\sqrt{\frac{Ux}{\nu}} = \sqrt{\bar{x}} \tag{8.36}$$

This shows that for $\bar{x} = 0$ both λ_1 and λ_2 are zero and hence the multimoment method reproduces the exact result that at $\bar{x} = 0$ the boundary layer starts as that for the flat plate without suction.

It can easily be shown that for $\lambda_1 = 0$ and $\lambda_2 = \sqrt{\bar{x}}$ a solution of equations (7.61) to (7.66) for all $N \geqslant 2$ is

$$\left.\begin{aligned} a_o &= \bar{x} \\ a_1 &= -2\bar{x} \\ a_2 &= \bar{x} \\ a_n &= 0 \qquad \text{for } n \geqslant 3 \end{aligned}\right\} \tag{8.37}$$

With (7.60) this leads to

$$S = \bar{\tau}^2 = \bar{x}(1-\bar{u})^2 \tag{8.38}$$

or $$\frac{\partial \bar{u}}{\partial \frac{y}{x}\sqrt{\frac{Ux}{\nu}}} = \bar{\tau} = \sqrt{\bar{x}}(1-\bar{u}) \tag{8.39}$$

After integration of (8.39) and using (8.27) it is found that

$$\bar{u} = 1 - e^{\frac{v_o y}{\nu}} \tag{8.40}$$

This reproduces the asymptotic suction profile discussed in section 3.1.5. Formally the solution (8.37) is valid from $\bar{x} = 0$ to $\bar{x} \to \infty$; however this would lead to the unrealistic solution $a_n = 0$ for $\bar{x} = 0$ discussed in section 8.2 for the flat plate without suction. Therefore it is expected that the solution (8.37) is only approached asymptotically for $\bar{x} \to \infty$; this is confirmed by further calculations, to be discussed below.

In view of (8.36) a new variable $z = \sqrt{\bar{x}}$ was used in the series method. Results of the series method for N = 7 are shown in fig. 8.25 where also results of a step by step calculation and the exact solution are shown.

Since $a_o \longrightarrow \bar{x}$ for large values of $\bar{x}$ it is advantageous to plot the quantity $\bar{x}/a_o$ versus $\sqrt{\bar{x}}$. This has been done in fig. 8.26 where results for N = 5, 6 and 7 are compared to the exact solution. In the same figure results of the momentum method have been included for comparison.

From the definitions of a_o and $\bar{x}$ (equation 8.27) it follows that

$$\frac{\bar{x}}{a_o} = \left[\frac{\frac{-v_o \delta^*}{\nu}}{\frac{\tau_o \delta^*}{\mu U}} \right]^2 \qquad (8.41)$$

and hence $\bar{x}/a_o$ can easily be found from the results of fig. 8.24.
It is seen from fig. 8.26 that the result of the multimoment method converges well to the exact solution for increasing N. The accuracy for N = 7 is comparable to that of the momentum method. The advantage of the multimoment method is that its accuracy can be improved by increasing N; results for N = 8 are very close to the exact solution.

8.12. Rheinboldt's boundary layer on a flat plate with discontinuous suction.

8.12.1. General.

Rheinboldt [86] designed a special procedure for the calculation of suction boundary layers with discontinuities in the suction velocity; the method was illustrated with several examples.
The first example discusses the boundary layer on a flat plate with non-porous entry length c followed by a porous region with constant suction for $x > c$ (see fig. 8.27a).
In a second example there is only suction for $c < x < 1.15c$ with a suction velocity v_o given by $\frac{-v_o}{U}\sqrt{\frac{Uc}{\nu}} = 1.5$ (see fig. 8.27b). In what follows c and U will be used as reference length and velocity and hence

$$\bar{x} = \frac{x}{c} \quad \text{and} \quad \bar{U} = 1 \qquad (8.42)$$

8.12.2. The momentum method.

The momentum method is found to be unable to cope with large discontinuities in the suction velocity; this may be seen as follows.
For the present case of zero pressure gradient only one independent parameter occurs in the momentum method (see chapter 5); it is convenient to select $\Lambda_2 = \frac{-v_o \theta}{\nu}$ for this parameter.

For the non-porous entry length the flat plate boundary layer without suction occurs which is represented by $\Lambda_2 = 0$. From this solution it is known that $\frac{\theta}{x}\sqrt{\frac{Ux}{\nu}} = 0.661$ (see table 5.1) and hence $\bar{\theta} = \frac{\theta}{c}\sqrt{\frac{Uc}{\nu}} = 0.661$ at $\bar{x} = 1$.

At discontinuities in v_o the momentum loss thickness θ is supposed to be continuous and hence directly downstream of $\bar{x} = 1$ it is found that

$$\Lambda_2 = \bar{v}_o.\bar{\theta} = 0.661\ \bar{v}_o$$

If the suction velocity has such a magnitude that $\bar{v}_o = \frac{0.50}{0.661}$ it follows that $\Lambda_2 = 0.50$; this implies that directly downstream of $\bar{x} = 1$ suddenly the asymptotic suction profile would be established. (compare also section 8.11). It can be expected however that in reality the boundary layer will only gradually approach asymptotic conditions.
Similarly the momentum method produces the erroneous result that the boundary layer velocity profile immediately returns to the Blasius shape if the suction is suddenly stopped at some station.
The way in which the boundary layer develops according to the momentum method can easily be calculated as follows.

From $\bar{U} = 1$

$$\Lambda_2 = \frac{-v_o\theta}{\nu} = \bar{v}_o \cdot \bar{\theta}$$

$$\Lambda_1 = 0$$

and $$\bar{v}_o = \frac{-v_o}{U}\sqrt{\frac{Uc}{\nu}} = \text{constant}$$

(8.44)

it is found that the momentum equation (5.18) can be written in the form

$$\bar{v}_o^{\,2}\, d\bar{x} = \frac{\Lambda_2}{2-\Lambda_2}\, d\Lambda_2 \qquad (8.45)$$

or after integration

$$\bar{v}_o^{\,2}\,(\bar{x}-1) = \int_{0.661\bar{v}_o}^{\Lambda_2} \frac{\Lambda_2}{2-\Lambda_2}\, d\Lambda_2 \qquad (8.46)$$

The integration constant in (8.46) has been chosen in such a way that for $\bar{x} = 1$ the suction parameter Λ_2 has the value 0.661 $\bar{v}_o$ (see equation 8.43). Values of the shape factor H, as determined from equation 8.46; for different values of $\bar{v}_o$ are shown in fig. 8.28 and compared to available results from Rheinboldt's calculation. It is seen that the momentum method is very inaccurate directly downstream of large discontinuities in the suction velocity.

.12.3. The multimoment method.

To check the accuracy of the multimoment method for discontinuously varying suction velocity only Rheinboldt's second example will be used. This is the most severe case of the two since here suction is started suddenly at $\bar{x} = 1$ and stopped again at $\bar{x} = 1.15$.
In the non-porous entry length $\bar{x} < 1$ the flat plate boundary layer without suction, discussed in section 8.2, is found. Hence table 8.1 provides the starting values at $\bar{x} = 1$ for the step by step solution. Since the boundary layer changes very rapidly near $\bar{x} = 1$ very small steps had to be used in this region. Fig. 8.29 shows a_o in the suction region for N = 5, 6 and 7; also the exact solution is given in the figure. It is seen that the results for N = 5 and 6 are not very accurate; those for N = 7 agree with the exact solution within the accuracy to which Rheinboldt's results can be read from the graphs in [86].
For the non-porous region downstream of $\bar{x} = 1.15$ only results for N = 7 are shown; a reasonably good correspondence with the exact solution is obtained. It should be noted that far downstream of the porous region again $a_o \longrightarrow 0.106$ which is the value obtained for the flat plate without suction.

.13. Schubauer's elliptic cylinder.

.13.1. General.

A detailed experimental observation of the laminar boundary layer on an elliptic cylinder has been made by Schubauer [25]. The lengths of the

major and minor axes of the cylinder were 11.78 and 3.98 inches respectively. The cylinder was placed in a wind tunnel with its major axis parallel to the flow. The measurements were performed at a windspeed of 11.5 ft/sec which resulted in the low value 72000 for the Reynolds number R_c based on the length of the major axis.

The pressure distribution around the cylinder was measured by means of orifices in the surface. Velocity profiles in the boundary layer were determined using hot wires. From the experiments Schubauer concluded that separation occurred at $\bar{x} = 1.99 \pm 0.02$ where $\bar{x} = x/c$ and c is the length of the minor axis of the cylinder. It was shown by Schubauer that application of Pohlhausen's method to the observed pressure distribution failed to show separation. Later an accurate numerical solution of the boundary layer equations for the observed pressure distribution was obtained by Hartree [26]. Again the theoretical results did not show separation. However, it was also shown by Hartree that a slight modification of the observed pressure distribution was sufficient to predict separation near $\bar{x} = 1.99$.

Due to the uncertainty about the experimentally determined pressure distributions to be used for the calculations it has - for so far the author knows - never been shown conclusively whether or not the boundary layer equations will be able to predict separation for experimentally determined pressure distributions.

In chapter 10 some new measurements will be described which - in agreement with Schubauer's data - show that it is very difficult to assess the validity of the boundary layer equations close to separation from measured pressure distributions. In the next section some results will be presented of calculations with the momentum method and the multimoment method for Schubauer's observed pressure distribution and for the modified distribution.

8.13.2. Results of boundary layer calculations.

Calculations have been made with both new methods for the observed and the modified pressure distribution. To facilitate the computations, values of $\bar{U}$ and $\frac{d\bar{U}}{d\bar{x}}$ taken from [26] have been plotted on a large scale. Then $\bar{U}$ and $\frac{d\bar{U}}{d\bar{x}}$ have been read from the graph for equidistant values of $\bar{x}$;

the results have been colledted in table 8.7. In the table also values for $\lambda_1 = \frac{\bar{x}}{\bar{U}} \frac{d\bar{U}}{d\bar{x}}$, to be used in the multimoment method, are given.
It has been shown by Hartree that near the stagnation point ($\bar{x} = 0$) the values of $\bar{U}$ can be approximated by

$$\bar{U} = 8.7\ \bar{x} - 24\ \bar{x}^2 + 24\ \bar{x}^3 + \ldots. \qquad (8.47)$$

which leads to the following expression for λ_1

$$\lambda_1 = 1 - 2.75862\ \bar{x} - 2.0927\ \bar{x}^2 + 1.837\ \bar{x}^3 + 10.84\ \bar{x}^4 + 24.8\ \bar{x}^5 + \ldots. \qquad (8.48)$$

To facilitate calculations with the multimoment method the values of λ_1 further downstream have been approximated by polynomial expressions of the form

$$\lambda_1 = \sum_{n=0}^{6} e_n \bar{x}^n \qquad (8.49)$$

The coefficients e_n have been collected in table 8.8. Fig. 8.30 shows the functions $\bar{U}$, $\frac{d\bar{U}}{d\bar{x}}$ and λ_1 in graphical form.

Results of boundary layer calculations with the momentum method and the multimomentmethod are presented in figs 8.31 to 8.32. Fig. 8.31 shows a_o for the observed pressure distribution according to the momentum method and to the multimoment method for N = 7. Results for N = 5 and 6 are close to those for N = 7 and therefore are not shown in the figure. The same curves are drawn to a larger scale in fig. 8.32 for $1.6 \leqslant \bar{x} \leqslant 2.10$; now also results of the multimoment method for N = 5 and 6 are included.
It can be concluded that the results of the multimoment method for increasing N converge well to Hartree's solution. The accuracy of the momentum method is somewhat less than for the multimoment method at N = 7. However, all methods agree in this respect that they do not show separation.
Similar results for the modified pressure distribution are included.

in fig. 8.32. It is noticed that the momentum method predicts separation at $\bar{x} = 1.92$ as compared to 1.983 for Hartree's calculation and 1.99 ± 0.02 for the experiment. As usual the multimoment method gives no clear indication of separation.

However, if the results for N = 6 and 7 are extrapolated using equation (8.1) the resulting curve comes very close to Hartree's values until near separation.

8.14. Concluding remarks on the new calculation methods.

From the examples discussed in the present chapter the following conclusions may be drawn.

1. The momentum method leads to accurate results as long as no large discontinuities in the suction velocity occur.
2. The accuracy of the multimoment method for N = 7 or 8 is comparable to or better than the accuracy of the momentum method. If discontinuities in the suction velocity occur, the multimoment method retains its accuracy while the momentum method (and all comparable methods) will fail.
3. A more rapid convergence of the multimoment method with increasing N would be desirable near separation.
4. A disadvantage of the multimoment method in the case of no suction is the following.

For the no-suction case $\lambda_2 = 0$ and hence equation (7.61) reduces to

$$\bar{x} \frac{da_o}{d\bar{x}} = a_o(1 - 3\lambda_1 + 6\, a_3) \qquad (8.50)$$

This equation shows that near separation where $a_o \longrightarrow 0$ also $\frac{da_o}{d\bar{x}}$ will tend to zero unless $\left|1 - 3\lambda_1 + 6\, a_3\right|$ tends to infinity.

From the results presented in this chapter it may be noticed that indeed $\frac{da_o}{d\bar{x}} \longrightarrow 0$ near separation making it difficult to give an accurate estimate of the position of separation. For some examples (see for instance figs 8.20 and 8.23) it is observed that the curve for a_o bends sharply into the $\bar{x}$-axis especially at high values of N so that

the position of separation can easily be determined from a short extrapolation of the straight part of the curve.

It is suggested by these results that for $N \rightarrow \infty$ the derivative $\frac{da_o}{d\bar{x}}$ may tend to a constant non-zero value when separation is approached. This would be in agreement with Goldstein's theory [84]. Equation (8.61) shows that in this case $\left| 1-3\lambda_1 + 6\, a_3 \right|$ has to approach infinity near separation. As an example fig. 8.33 shows $-(1-3\lambda_1 + 6a_3)$ as function of $\bar{x}$ and a_o for $\bar{U} = \sin \bar{x}$ near separation. It is found indeed that $-(1-3\lambda_1 + 6a_3)$ becomes very large for $a_o \rightarrow 0$.

In view of these remarks it seems to be worth while to inquire whether the results near separation can be improved by omitting equation (7.61) and replacing it by an additional moment equation.

The modification will slightly complicate the application of the method for the case of suction since then the non-linear factor $\sqrt{a_o}$ appears as unknown parameter in equations (7.62) and (7.63). This possible modification of the method will not be pursued further in the present work however.

Table 8.1: The coefficients a_n for the flat plate without suction; $a_1 = a_2 = 0$, $a_3 = -1/6$

N	a_o	a_4	a_5	a_6	a_7	a_8	a_9
4	0.041666	+0.125000	-	-	-	-	-
5	0.100602	-0.169677	+0.235742	-	-	-	-
6	0.102937	+0.193777	-0.505175	+0.375128	-	-	-
7	0.106509	-0.227102	+0.995693	-1.388978	+0.680544	-	-
8	0.107822	+0.250871	-1.637534	+3.871663	-3.863447	+1.437293	-
9	0.108526	-0.263250	+2.395702	-8.149445	+13.338101	-10.471178	+3.208202

Table 8.2: Some characteristic parameters for the boundary layer on a flat plate without suction according to the multimoment method.

N	a_o	%	$\frac{\delta^*}{x}\sqrt{\frac{Ux}{\nu}}$	%	$\frac{\theta}{x}\sqrt{\frac{Ux}{\nu}}$	%	$H = \frac{\delta^*}{\theta}$	%	$\lambda = \frac{\tau_o \Theta}{\mu U}$	(%)
4	0.041666	37.8	3.123	181.5	1.3260	199.7	2.356	90.9	0.2707	122.7
5	0.100602	91.2	1.918	111.5	0.7882	118.7	2.433	93.9	0.2500	113.4
6	0.102937	93.4	1.822	105.9	0.7248	109.1	2.514	97.0	0.2325	105.4
7	0.106509	96.6	1.779	103.4	0.7001	105.4	2.541	98.1	0.2285	103.6
8	0.107822	97.8	1.758	102.2	0.6879	103.6	2.556	98.7	0.2259	102.4
9	0.108526	98.4	1.748	101.6	0.6817	102.6	2.565	99.0	0.2246	101.8
7*	0.110081	99.8	1.741	101.1	0.6791	102.3	2.563	98.9	0.2253	102.2
exact, Smith[14]	0.110262	100.0	1.721	100.0	0.6641	100.0	2.591	100.0	0.2205	100.0

Table 8.3: The coefficients a_n for the plane stagnation point without suction; $a_1 = -2$, $a_2 = 0$, $a_3 = +1/3$.

N	a_o	a_4	a_5	a_6	a_7	a_8	a_9
4	1.416667	+0.250000	-	-	-	-	-
5	1.498997	-0.161653	0.329322	-	-	-	-
6	1.510251	+0.296525	-0.654560	+0.514450	-	-	-
7	1.514489	-0.204411	+1.274888	-1.871296	+0.952997	-	-
8	1.516397	+0.328998	-1.904711	+4.852614	-5.104930	+1.978298	-
9	1.517393	-0.230753	+2.833957	-10.120913	+17.328192	-14.132244	+4.471035

Table 8.4: Some characteristic parameters for the plane stagnation point without suction according to the multimoment method.

N	a_o	%	$\frac{\delta^*}{x}\sqrt{\frac{Ux}{\nu}}$	%	$\frac{\theta}{x}\sqrt{\frac{Ux}{\nu}}$	%	$H = \frac{\delta^*}{\theta}$	%	$\ell = \frac{\tau_o \theta}{\mu U}$	%
4	1.416667	93.3	0.7296	112.6	0.3475	118.9	2.099	94.7	0.4136	114.8
5	1.498997	98.7	0.6808	105.1	0.3179	108.7	2.142	96.6	0.3892	108.0
6	1.510251	99.4	0.6652	102.7	0.3066	104.9	2.169	97.9	0.3768	104.6
7	1.514489	99.7	0.6586	101.6	0.3014	103.1	2.185	98.6	0.3709	102.9
8	1.516397	99.8	0.6551	101.1	0.2986	102.1	2.194	99.0	0.3677	102.0
9	1.517393	99.9	0.6531	100.8	0.2969	101.6	2.200	99.3	0.3657	101.5
7*	1.518725	100.0	0.6525	100.7	0.2967	101.5	2.199	99.2	0.3656	101.5
exact, Smith [114]	1.519278	100.0	0.6479	100.0	0.2923	100.0	2.216	100.0	0.3603	100.0

Table 8.5: Some characteristic parameters for the Hartree boundary layer with $\beta = -0.16$.

N	a_o	%	$\frac{\delta^*}{x}\sqrt{\frac{Ux}{\nu}}$	%	$\frac{\theta}{x}\sqrt{\frac{Ux}{\nu}}$	%	$H = \frac{\delta^*}{\theta}$	%	$\ell = \frac{\tau_o \theta}{\mu U}$	%
5	0.012325	73.2	2.795	111.4	0.9452	116.5	2.957	95.7	0.1049	99.6
6	0.007625	45.3	2.905	115.8	0.9103	112.2	3.191	103.2	0.0795	75.5
7	0.014790	87.8	2.613	104.2	0.8553	105.4	3.055	98.8	0.1040	98.8
exact, Smith [114]	0.016850	100.0	2.508	100.0	0.8116	100.0	3.091	100.0	0.1053	100.0

Table 8.6: Separation positions for Tani's boundary layers $\bar{U} = 1 - \bar{x}^j$

method	$\bar{x}$ at separation for j =			
	1	2	4	8
exact	0.120	0.271	0.462	0.640
momentum method	0.123	0.264	0.446	0.621
multimoment method, N=7	0.121	0.268	0.465	0.648

Table 8.7: The pressure distribution used in the boundary layer calculations for Schubauer's elliptic cylinder.

$\bar{x}$	$\bar{U}$	$\frac{d\bar{U}}{d\bar{x}}$	λ_1
0.16	—	—	+0.5220
0.18	—	—	+0.4835
0.20	+0.966	+1.925	+0.4090
0.22	+1.002	+1.626	+0.3565
0.24	+1.031	+1.392	+0.3241
0.26	+1.057	+1.210	+0.2977
0.28	+1.080	+1.050	+0.2723
0.30	+1.100	+0.925	+0.2522
0.32	+1.118	+0.821	+0.2350
0.34	+1.133	+0.729	+0.2188
0.36	+1.147	+0.654	+0.2053
0.38	+1.160	+0.588	+0.1926
0.40	+1.171	+0.534	+0.1824
0.42	+1.180	+0.486	+0.1730
0.44	+1.190	+0.444	+0.1641
0.46	+1.198	+0.406	+0.1559
0.48	+1.206	+0.372	+0.1481
0.50	+1.213	+0.344	+0.1418
0.52	+1.220	+0.318	+0.1355
0.54	+1.226	+0.295	+0.1299
0.56	+1.232	+0.275	+0.1250
0.58	+1.237	+0.256	+0.1200
0.60	+1.242	+0.240	+0.1159
0.62	+1.247	+0.223	+0.1109
0.64	+1.251	+0.207	+0.1059
0.66	+1.255	+0.192	+0.1010
0.68	+1.258	+0.178	+0.0962
0.70	+1.262	+0.165	+0.0915
0.72	+1.265	+0.152	+0.0865
0.74	+ 1.268	+0.141	+0.0823
0.76	+1.270	+0.130	+0.0778
0.78	+1.273	+0.119	+0.0729
0.80	+1.275	+0.110	+0.0690
0.82	+1.278	+0.100	+0.0642
0.84	+1.280	+0.092	+0.0604
0.86	+1.281	+0.084	+0.0564
0.88	+1.283	+0.077	+0.0528
0.90	+1.285	+0.070	+0.0490
0.92	+1.286	+0.064	+0.0458
0.94	+1.287	+0.057	+0.0416
0.96	+1.288	+0.051	+0.0380
0.98	+1.289	+0.046	+0.0350
1.00	+1.290	+0.040	+0.0310
1.02	+1.291	+0.036	+0.0284
1.04	+1.292	+0.032	+0.0258
1.06	+1.293	+0.029	+0.0238
1.08	+1.294	+0.026	+0.0217
1.10	+1.294	+0.023	+0.0196
1.12	+1.294	+0.020	+0.0173
1.14	+1.295	+0.018	+0.0158
1.16	+1.295	+0.016	+0.0143
1.18	+1.295	+0.014	+0.0128
1.20	+1.295	+0.012	+0.0111
1.22	+1.295	+0.009	+0.0085
1.24	+1.295	+0.006	+0.0057
1.26	+1.295	+0.003	+0.0029
1.28	+1.295	+0.000	+0.0000
1.30	+1.295	-0.003	-0.0030
1.32	+1.295	-0.006	-0.0061
1.34	+1.295	-0.009	-0.0093
1.36	+1.295	-0.013	-0.0136
1.38	+1.295	-0.017	-0.0181
1.40	+1.295	-0.021	-0.0227
1.42	+1.295	-0.026	-0.0285
1.44	+1.294	-0.031	-0.0345
1.46	+1.293	-0.036	-0.0407
1.48	+1.292	-0.042	-0.0481
1.50	+1.291	-0.047	-0.0546
1.52	+1.290	-0.053	-0.0624
1.54	+1.289	-0.058	-0.0693
1.56	+1.288	-0.064	-0.0775
1.58	+1.287	-0.070	-0.0859
1.60	+1.285	-0.076	-0.0946
1.62	+1.283	-0.082	-0.1035
1.64	+1.282	-0.087	-0.1113
1.66	+1.280	-0.093	-0.1206
1.68	+1.278	-0.098	-0.1288
1.70	+1.276	-0.102	-0.1359
1.72	+1.274	-0.106	-0.1431
1.74	+1.272	-0.110	-0.1505
1.76	+1.270	-0.113	-0.1566
1.78	+1.268	-0.115	-0.1614
1.80	+1.265	-0.117	-0.1665
1.82	+1.262	-0.118	-0.1702
1.84	+1.260	-0.119	-0.1738
1.86	+1.258	-0.119	-0.1759
1.88	+1.254	-0.118	-0.1769
1.90	+1.253	-0.118	-0.1789
1.92	+1.251	-0.117	-0.1796
1.94	+1.249	-0.115	-0.1786
1.96	+1.246	-0.113	-0.1777
1.98	+1.244	-0.110	-0.1750
2.00	+1.242	-0.107	-0.1723
2.02	+1.240	-0.104	-0.1694
2.04	+1.238	-0.100	-0.1648
2.06	+1.236	-0.095	-0.1583
2.08	+1.234	-0.090	-0.1517

Table 8.7: Continued; Modified pressure distribution.

$\bar{x}$	$\bar{U}$	$\frac{d\bar{U}}{d\bar{x}}$	λ_1
1.80	+1.265	-0.117	-0.1665
1.82	+1.262	-0.119	-0.1716
1.84	+1.260	-0.122	-0.1782
1.86	+1.258	-0.126	-0.1863
1.88	+1.254	-0.130	-0.1949
1.90	+1.2525	-0.133	-0.2018
1.92	+1.250	-0.136	-0.2089
1.94	+1.248	-0.138	-0.2145
1.96	+1.245	-0.140	-0.2204
1.98	+1.242	-0.142	-0.2264
2.00	+1.239	-0.143	-0.2308
2.02	+1.237	-0.145	-0.2368
2.04	+1.235	-0.146	-0.2412

Table 8.8: Coefficients e_n in equation (8,49) for Schubauer's ellips.

(0.35 + 2 denotes $0.35 \times 10^{+2}$).

n	$0.10 \leq \bar{x} < 0.50$	$0.50 \leq \bar{x} < 0.90$	$0.90 \leq \bar{x} < 1.30$	$1.30 \leq \bar{x} < 1.70$	$1.70 \leq \bar{x} < 2.10$	modified $1.80 \leq \bar{x} < 2.10$
0	+0.2229526 + 0	+0.878004 + 0	-0.344650 + 0	+0.118466 + 1	-0.272018 + 0	+0.482076 + 1
1	+0.1779934 + 2	-0.399223 + 1	+0.543894 + 0	-0.237210 + 1	+0.131212 + 1	-0.344721 + 1
2	-0.2101468 + 3	+0.891446 + 1	+0.370504 + 1	+0.714958 + 0	-0.565421 + 0	-0.273478 + 1
3	+0.1020643 + 4	-0.103245 + 2	-0.102364 + 2	+0.106592 + 1	-0.513816 + 0	+0.197142 + 1
4	-0.2526967 + 4	+0.583033 + 1	+0.970133 + 1	-0.335165 + 0	+0.246656 + 0	+0.997831 + 0
5	+0.3152842 + 4	-0.137626 + 1	-0.382806 + 1	-0.385864 + 0	+0.191498 - 1	-0.962272 + 0
6	-0.1575414 + 4	+0.107946 + 0	+0.490446 + 0	+0.152730 + 0	-0.111240 - 1	+0.184954 + 0

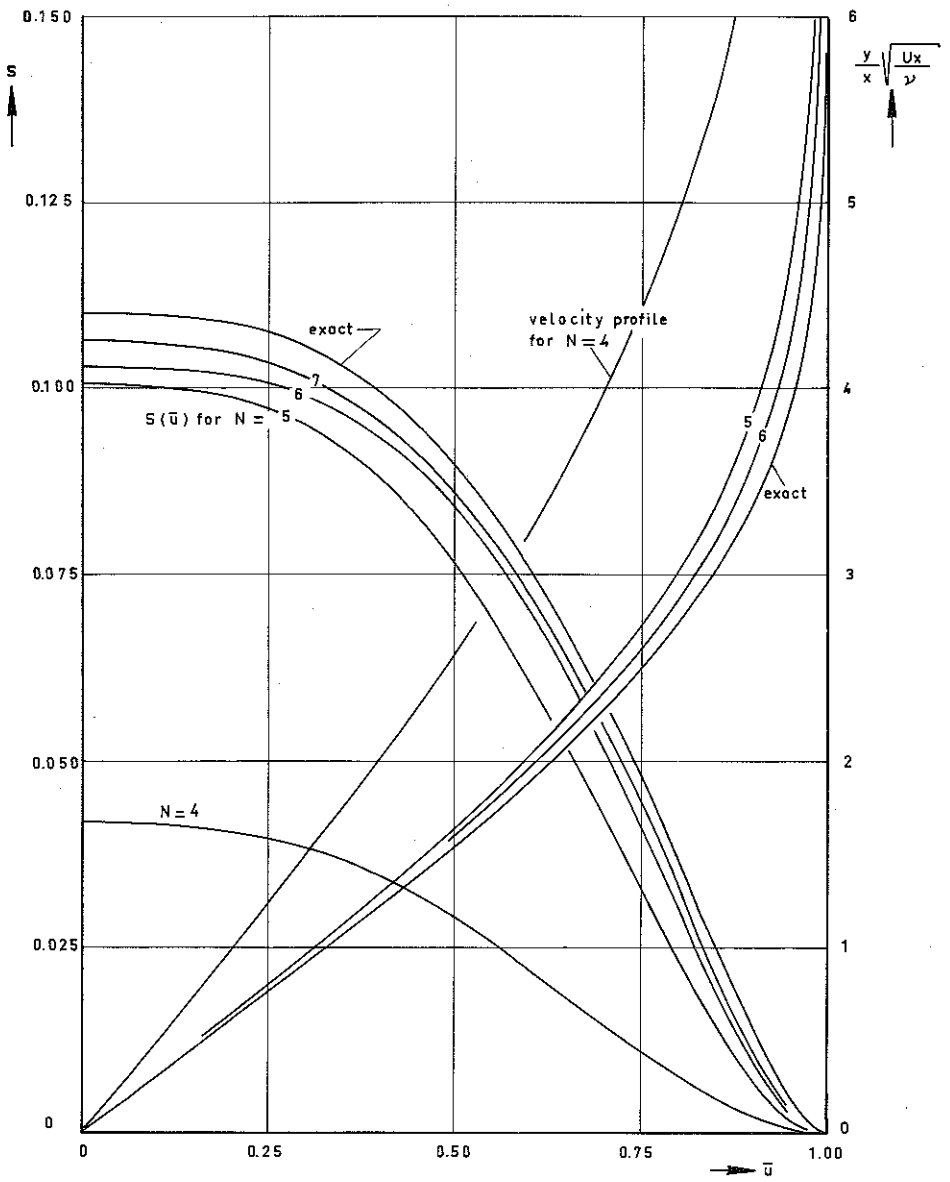

FIG. 8.1: S($\bar{u}$) AND VELOCITY PROFILES FOR THE FLAT PLATE WITHOUT SUCTION AT DIFFERENT VALUES OF N.

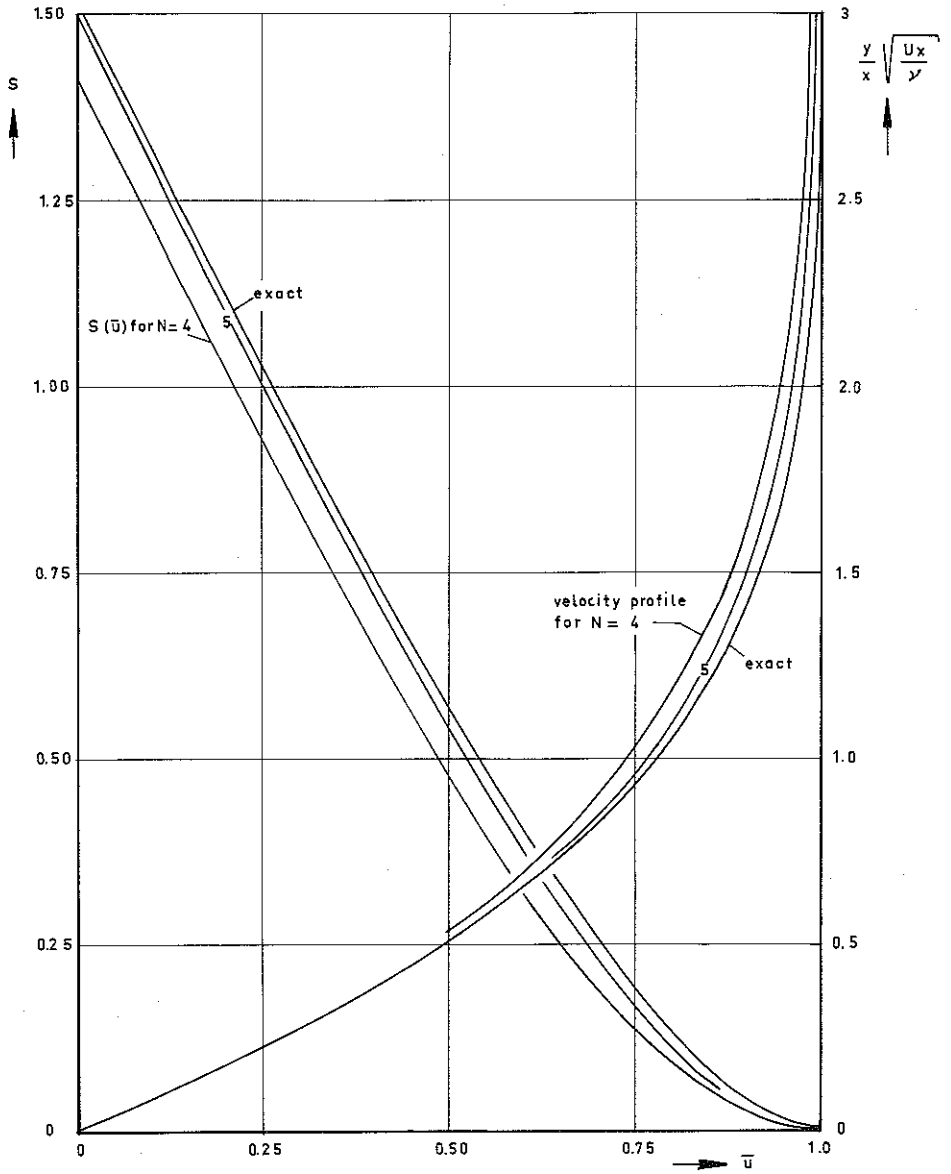

FIG. 8.2: S(ū) AND VELOCITY PROFILES FOR THE PLANE STAGNATION POINT WITHOUT SUCTION AT DIFFERENT VALUES OF N.

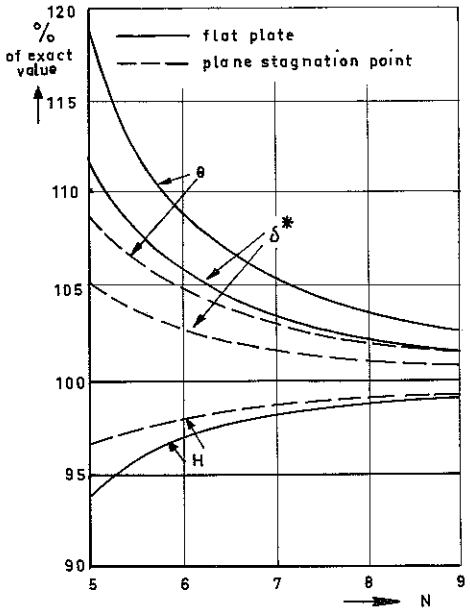

FIG. 8.3 : SOME RESULTS OF THE MULTIMOMENT METHOD FOR THE FLAT PLATE & STAGNATION POINT WITHOUT SUCTION.

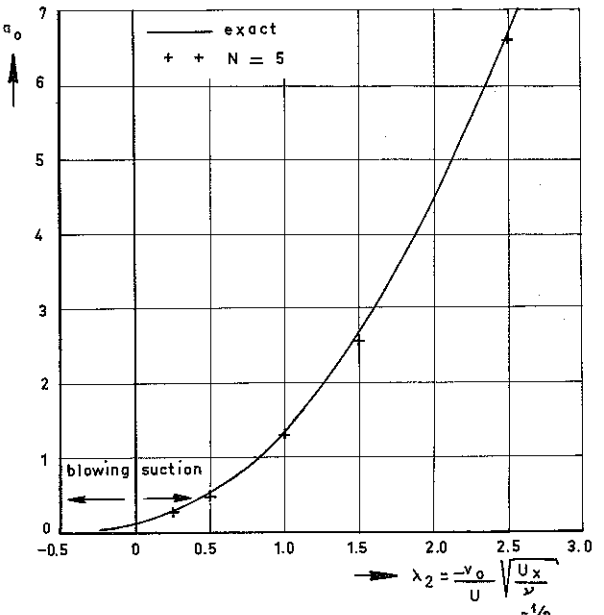

FIG. 8.4 : a_0 FOR THE FLAT PLATE WITH $v_0 \sim x^{-1/2}$

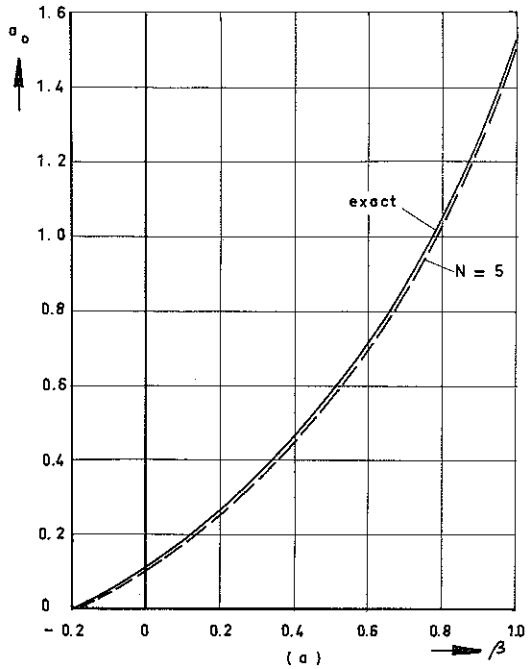

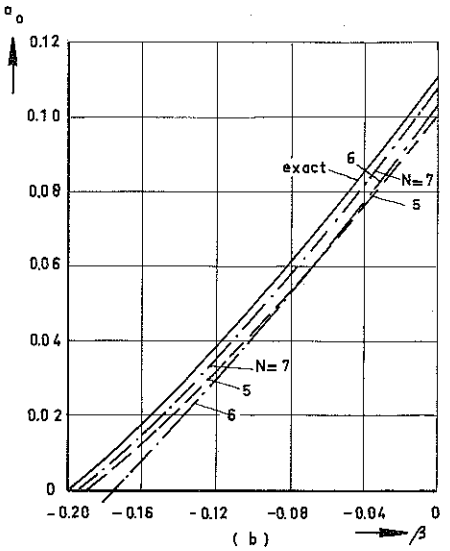

FIG. 8.5: a_0 FOR HARTREE'S BOUNDARY LAYERS WITHOUT SUCTION.

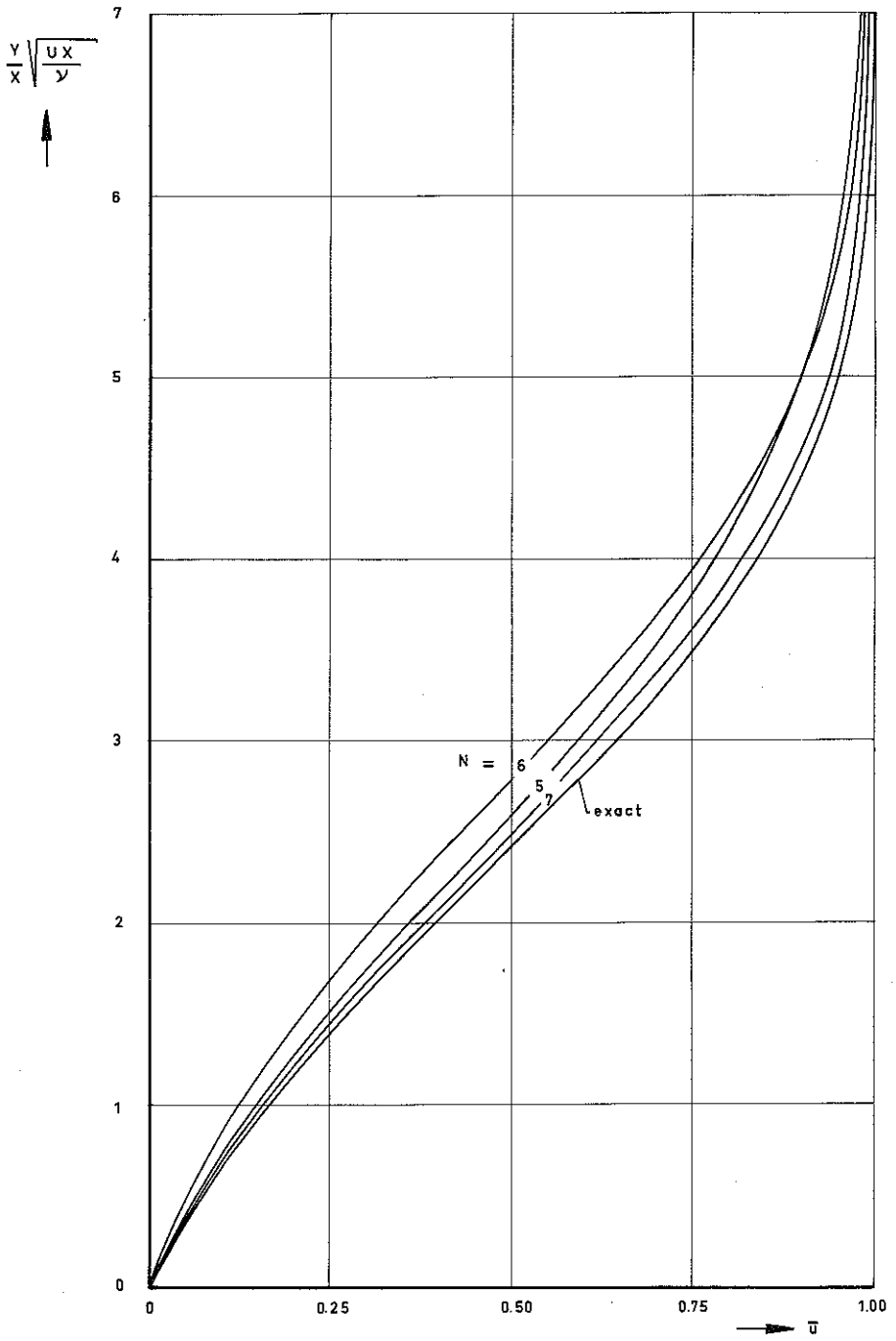

FIG. 8.6 : VELOCITY PROFILES FOR THE HARTREE BOUNDARY LAYER WITH $\beta = -0.15$

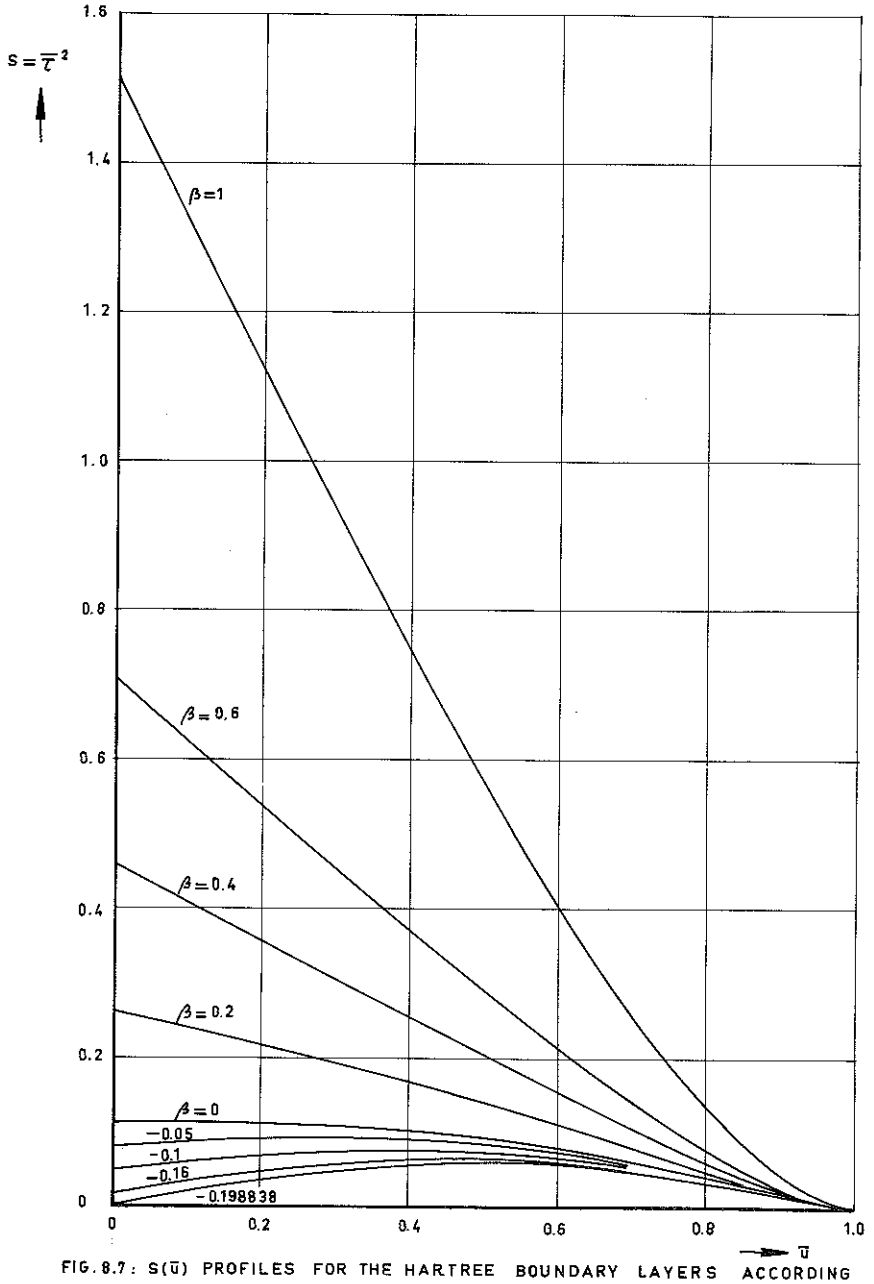

FIG. 8.7: $S(\overline{u})$ PROFILES FOR THE HARTREE BOUNDARY LAYERS ACCORDING TO THE EXACT SOLUTION BY SMITH [114].

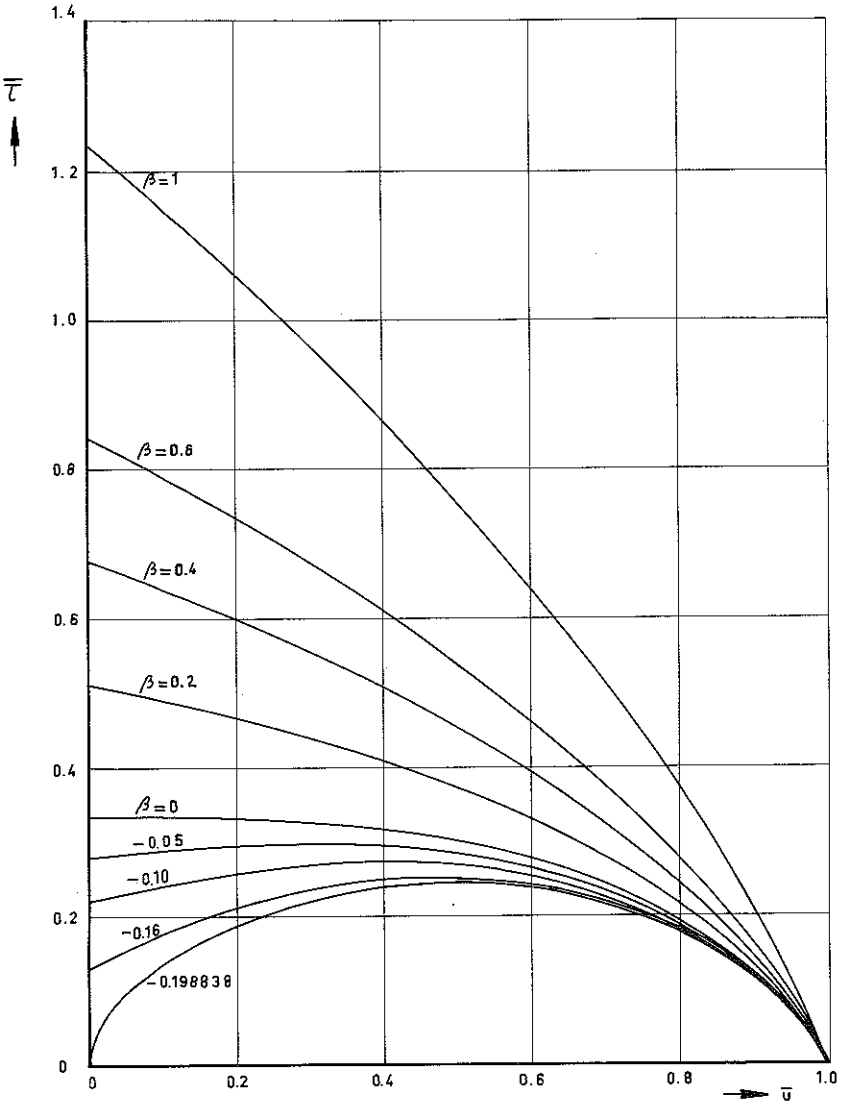

FIG. 8.8: SHEAR STRESS PROFILES FOR THE HARTREE BOUNDARY LAYERS ACCORDING TO THE EXACT SOLUTION BY SMITH [114]

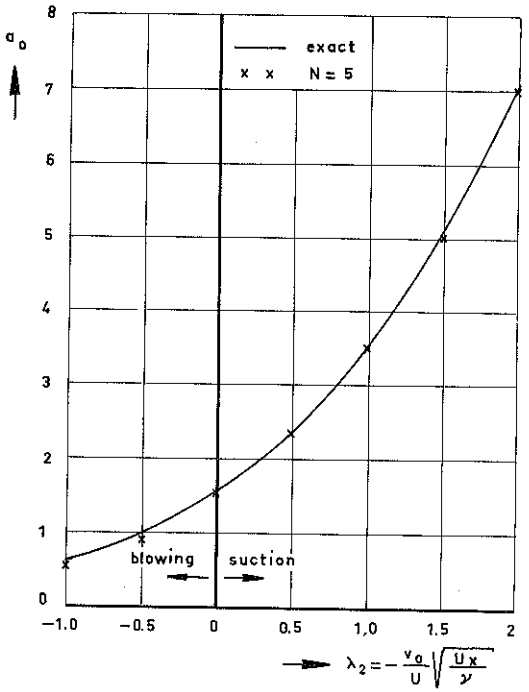

FIG. 8.9: a_0 FOR THE PLANE STAGNATION POINT WITH CONSTANT SUCTION VELOCITY.

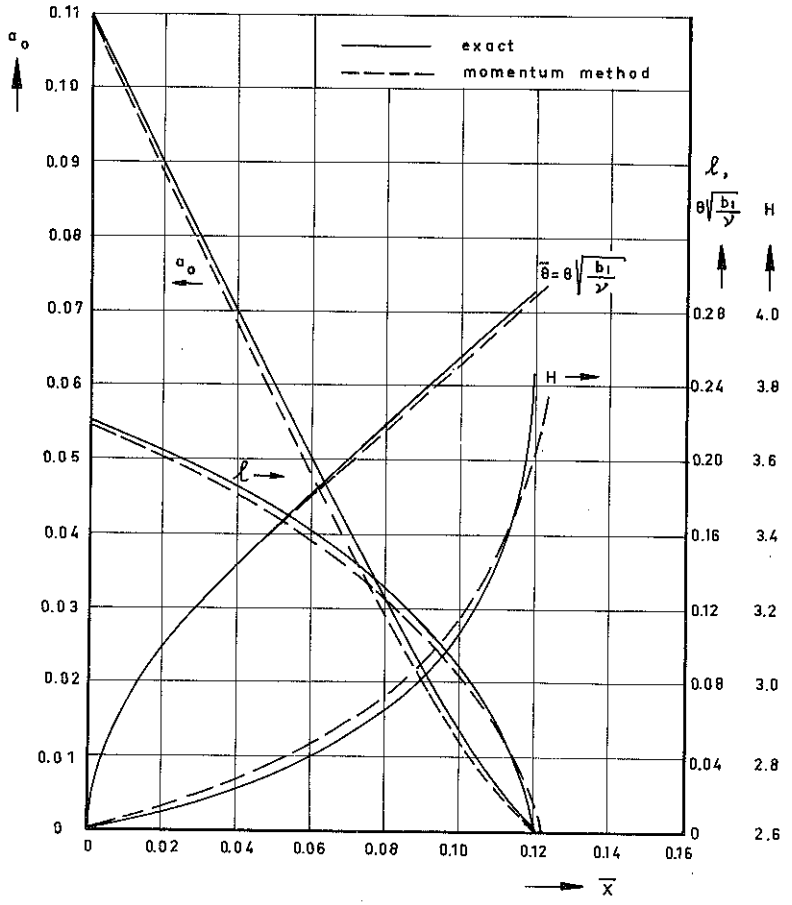

FIG. 8.10: RESULTS OF THE MOMENTUM METHOD FOR $\bar{U} = 1 - \bar{x}$.

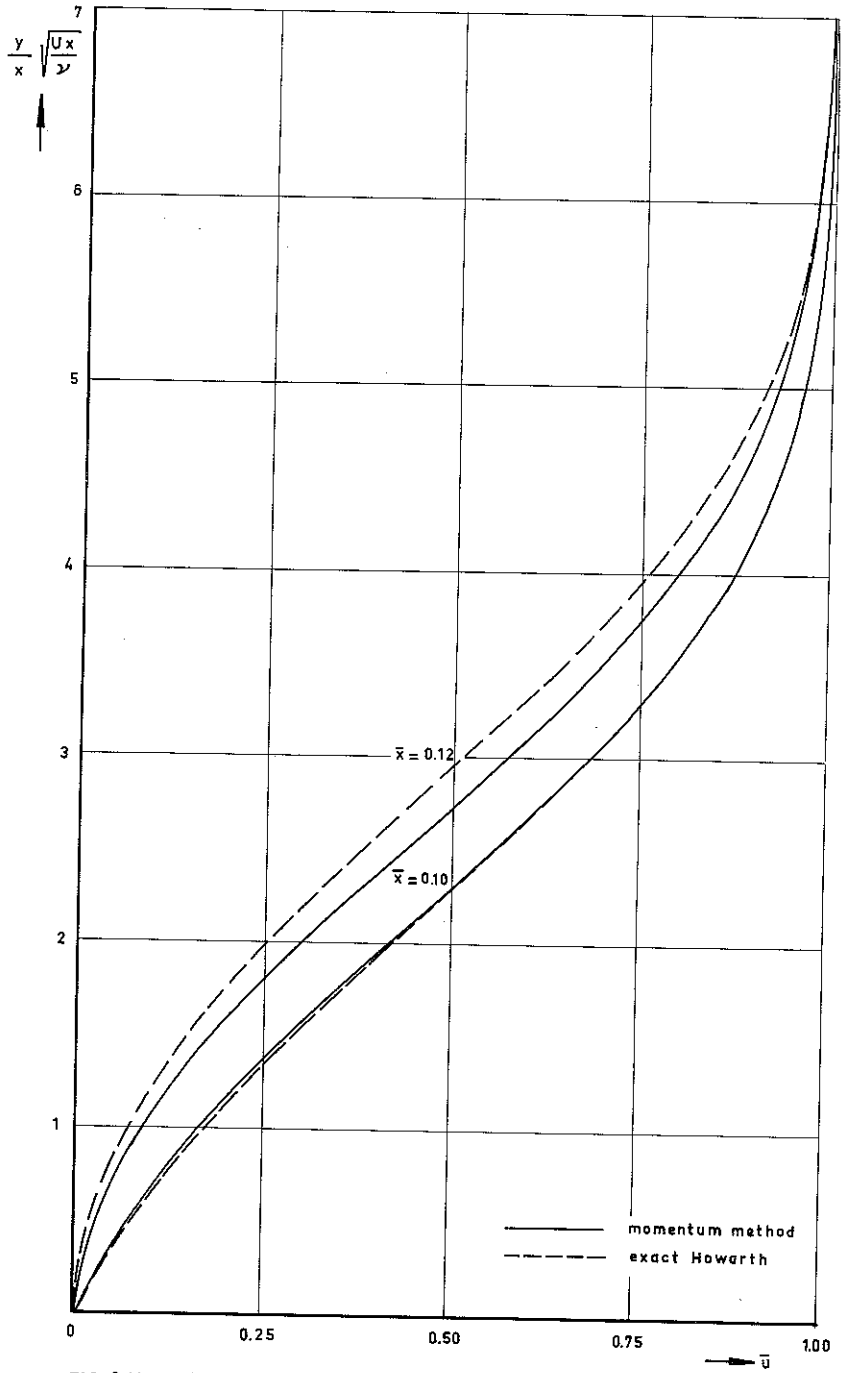

FIG. 8.11: VELOCITY PROFILES FOR $\bar{U} = 1 - \bar{x}$ AT $\bar{x} = 0.10$ AND 0.12 ACCORDING TO THE MOMENTUM METHOD.

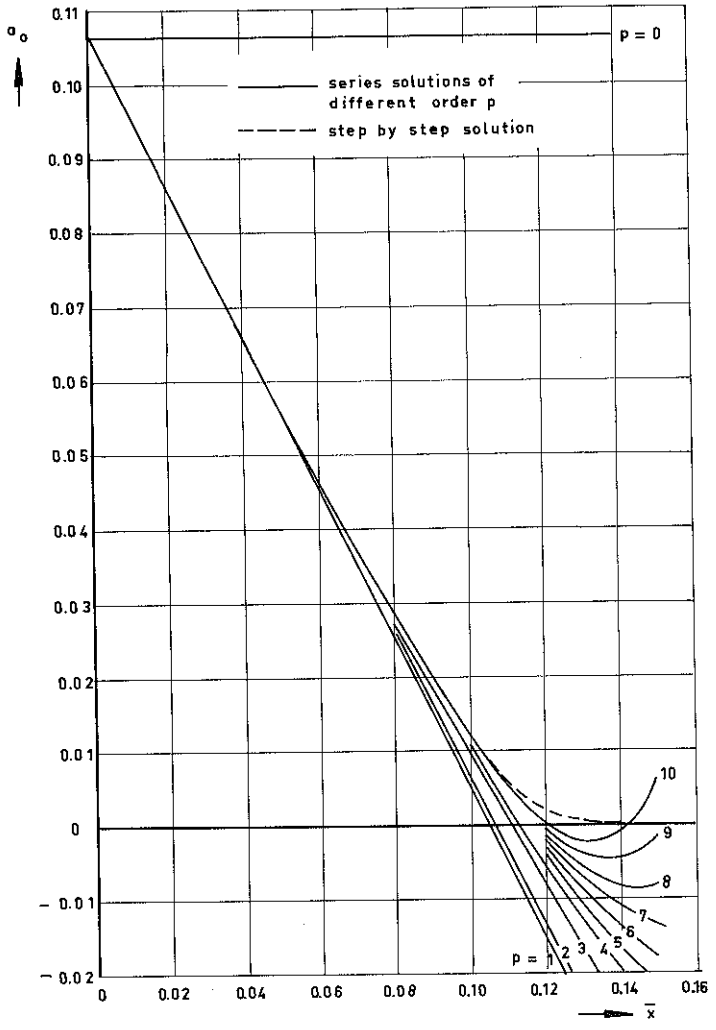

FIG. 8.12: THE MULTIMOMENT METHOD FOR $\bar{U} = 1 - \bar{x}$; N = 7

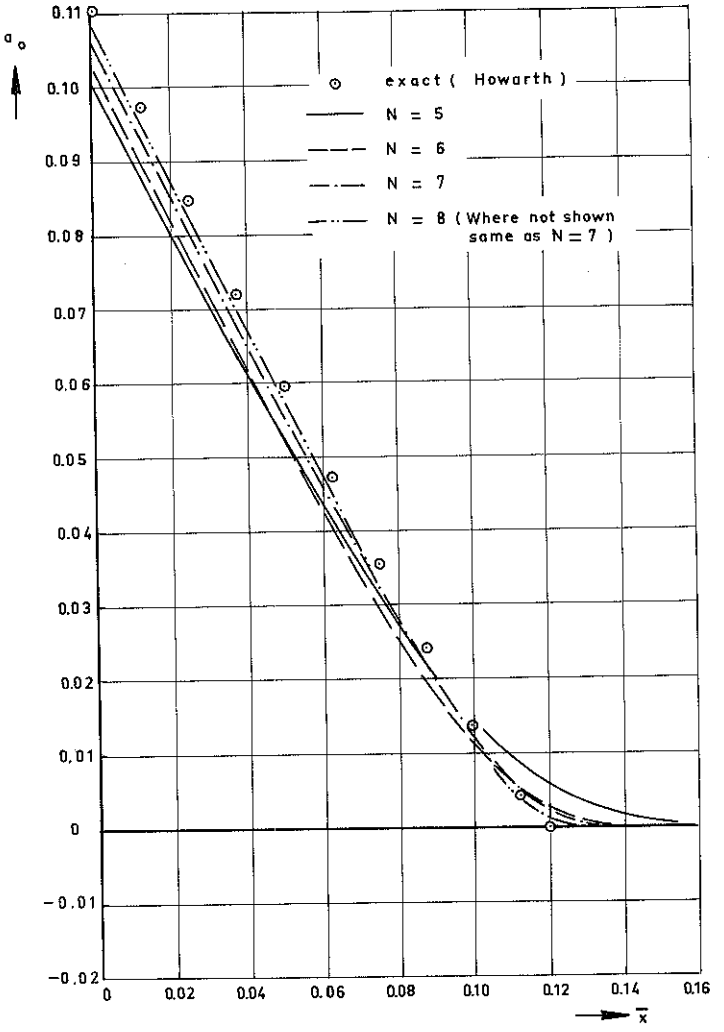

FIG. 8.13: a_o FOR $\bar{U} = 1 - \bar{x}$

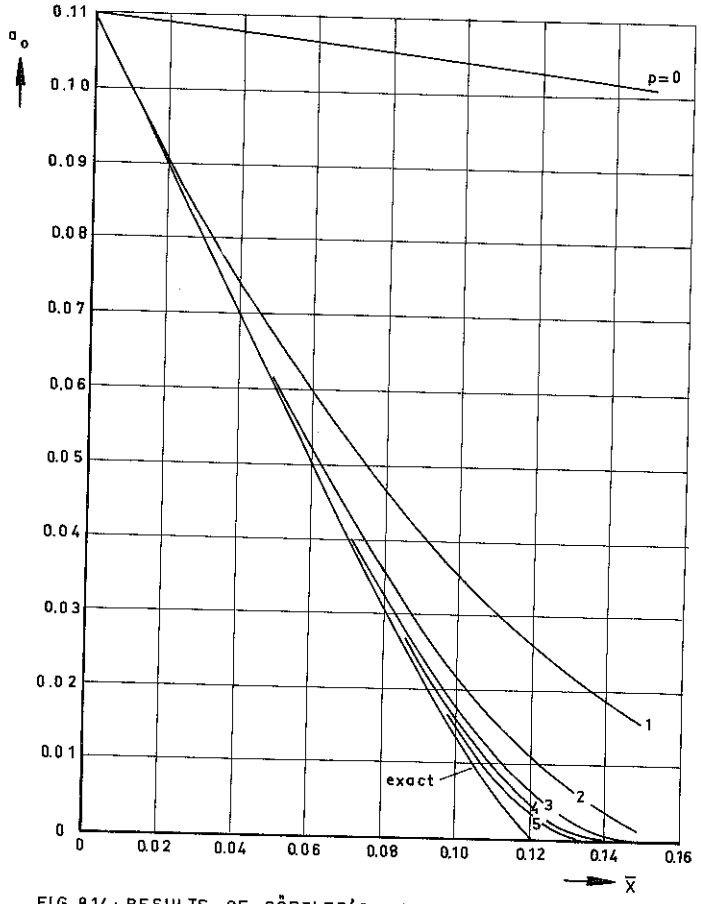

FIG. 8.14: RESULTS OF GÖRTLER'S SERIES METHOD FOR $\bar{U} = 1 - \bar{X}$

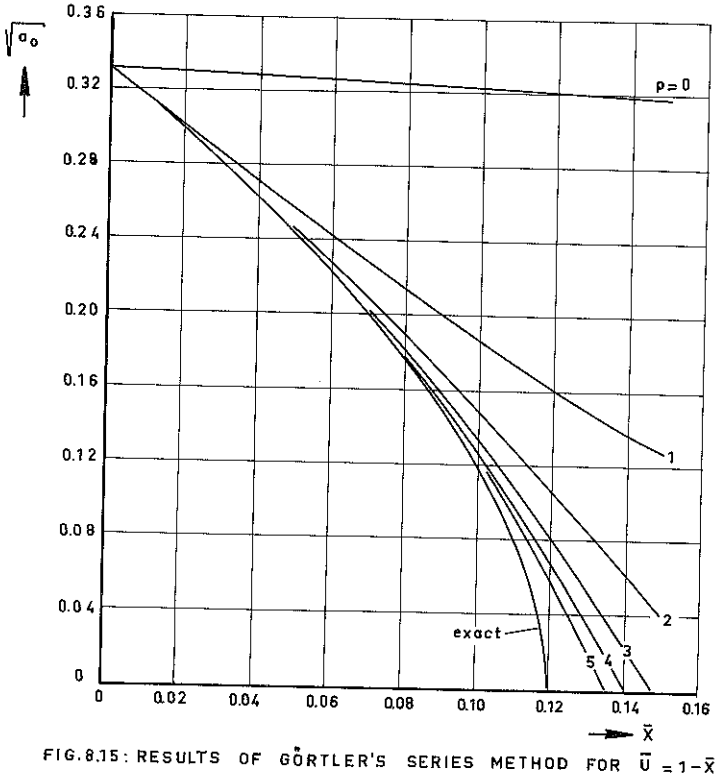

FIG. 8.15: RESULTS OF GÖRTLER'S SERIES METHOD FOR $\bar{U} = 1 - \bar{X}$

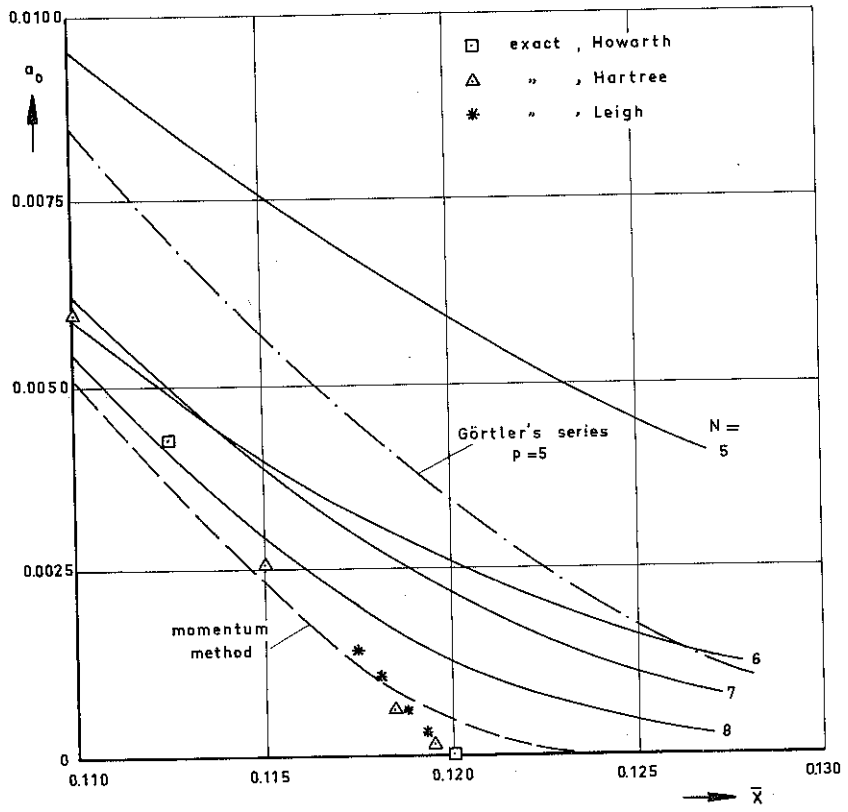

FIG. 8.16: a_0 NEAR THE SEPARATION POINT FOR $\bar{U} = 1 - \bar{x}$ ACCORDING TO DIFFERENT CALCULATION METHODS

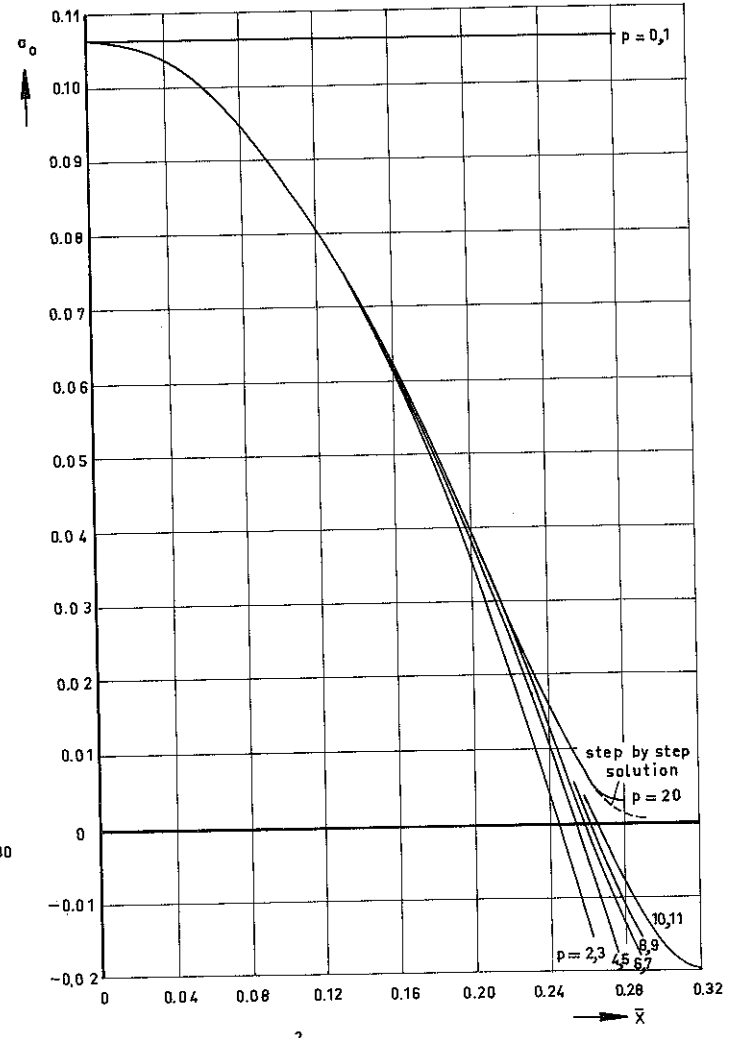

FIG. 8.17: a_0 FOR $\bar{U} = 1-\bar{x}^2$; N = 7

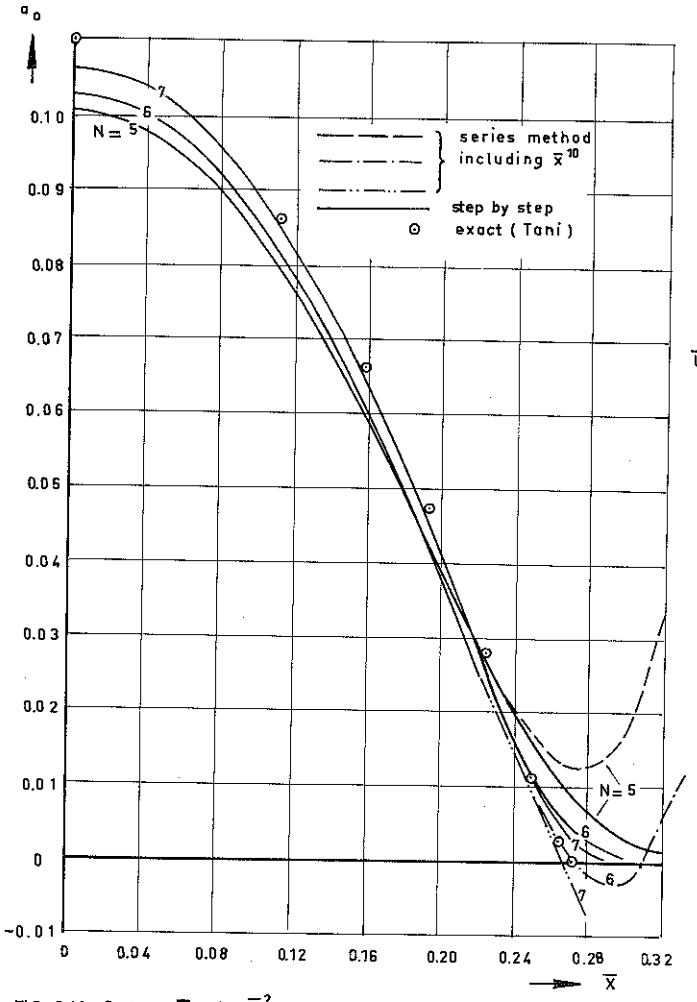

FIG. 8.18 : a_0 FOR $\bar{U} = 1 - \bar{X}^2$; MULTIMOMENT METHOD N = 5,6 AND 7

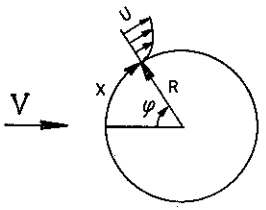

FIG. 8.19 : BOUNDARY LAYER ON A CIRCULAR CYLINDER.

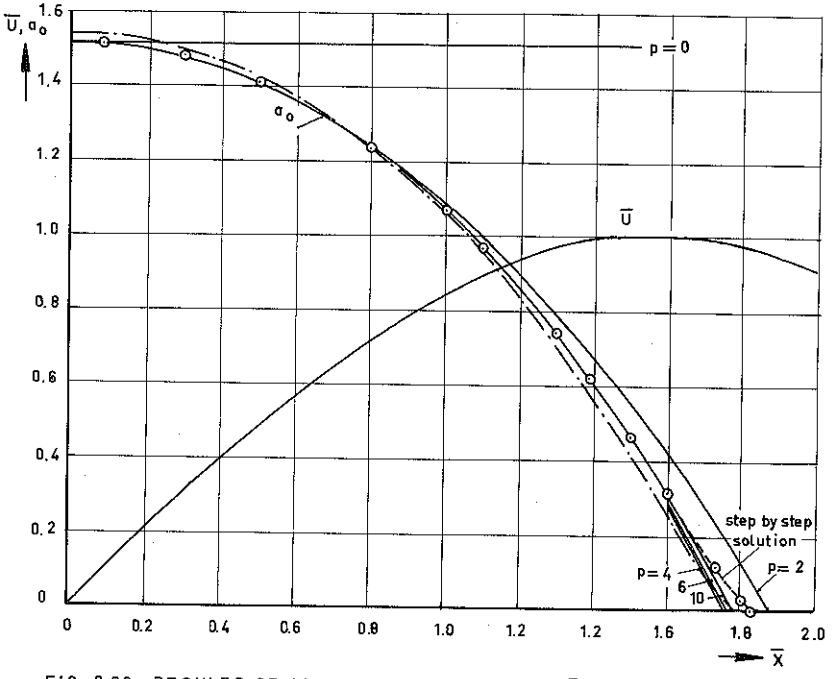

FIG. 8.20 : RESULTS OF DIFFERENT METHODS FOR $\bar{U} = \sin \bar{x}$.

⊙ ⊙ exact (Terrill)
——— multimoment method, N = 7 , series solution of order p.
– – – " " " , step by step solution
—·—·— momentum method

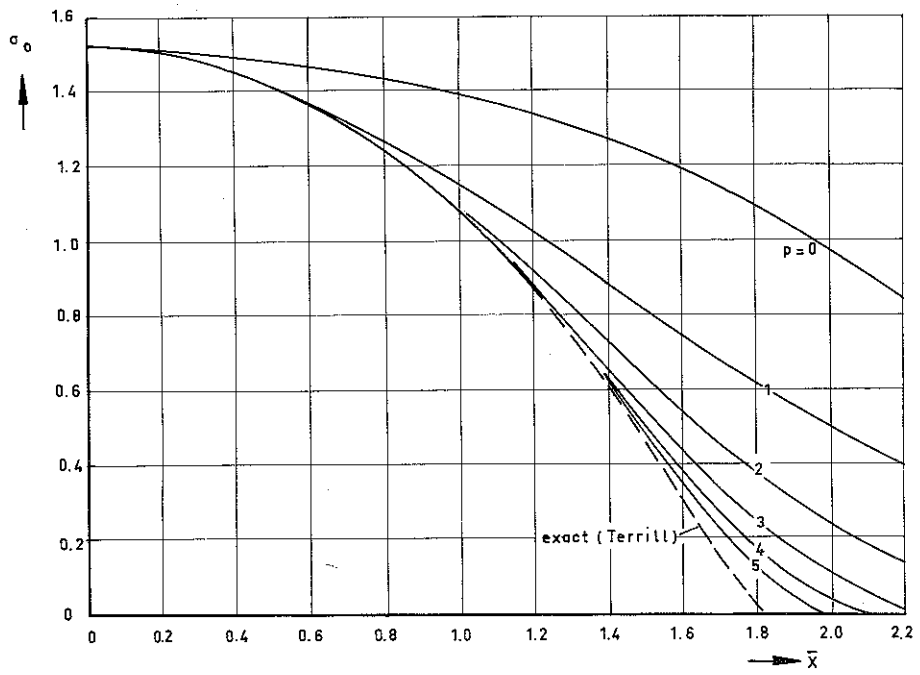

FIG. 8.21: a_0 ACCORDING TO GÖRTLER'S SERIES METHOD FOR $\bar{U} = \sin \bar{x}$

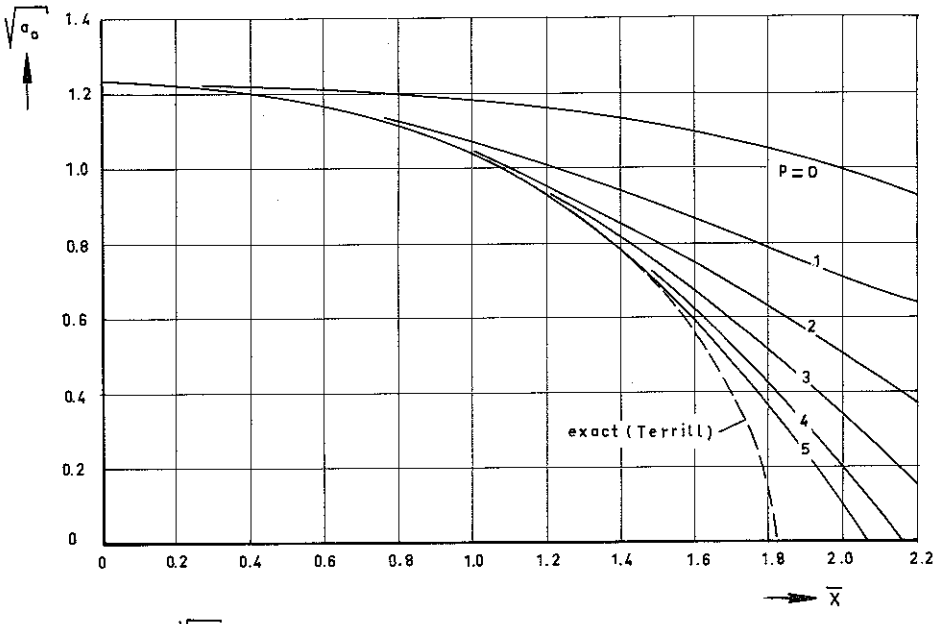

FIG. 8.22: $\sqrt{a_0}$ ACCORDING TO GÖRTLER'S SERIES METHOD FOR $\bar{U} = \sin \bar{x}$

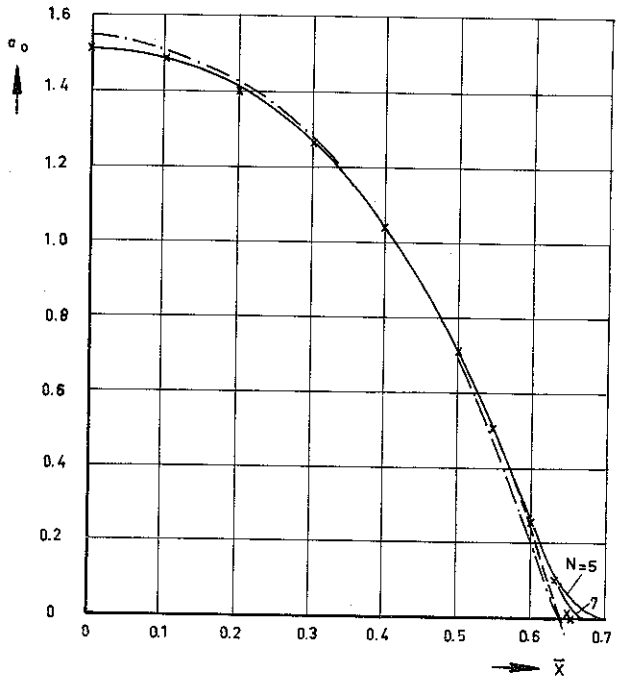

FIG. 8.23: RESULTS OF DIFFERENT METHODS FOR $\bar{U} = \bar{X} - \bar{X}^3$

x x x exact (Curle)

——— multimoment method, step bij step solution

– – – – " " , series solution, N = 7, p = 10

—·—·— momentum method

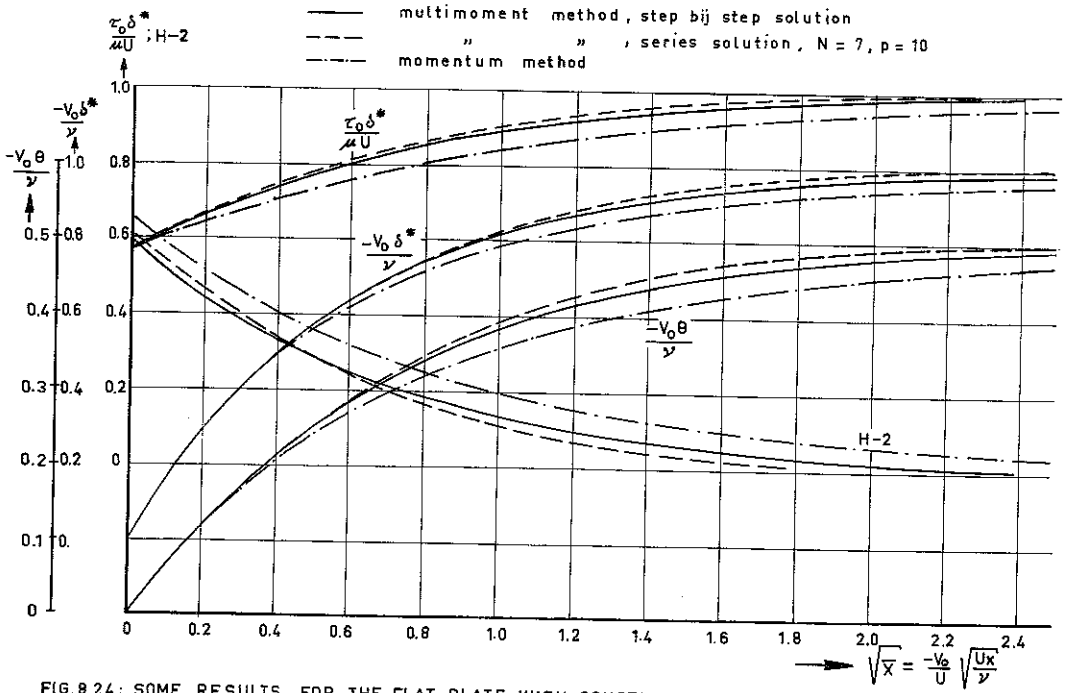

FIG. 8.24: SOME RESULTS FOR THE FLAT PLATE WITH CONSTANT SUCTION VELOCITY

——— exact. Iglisch

—·—·— Schlichting [55]

– – – – momentum method

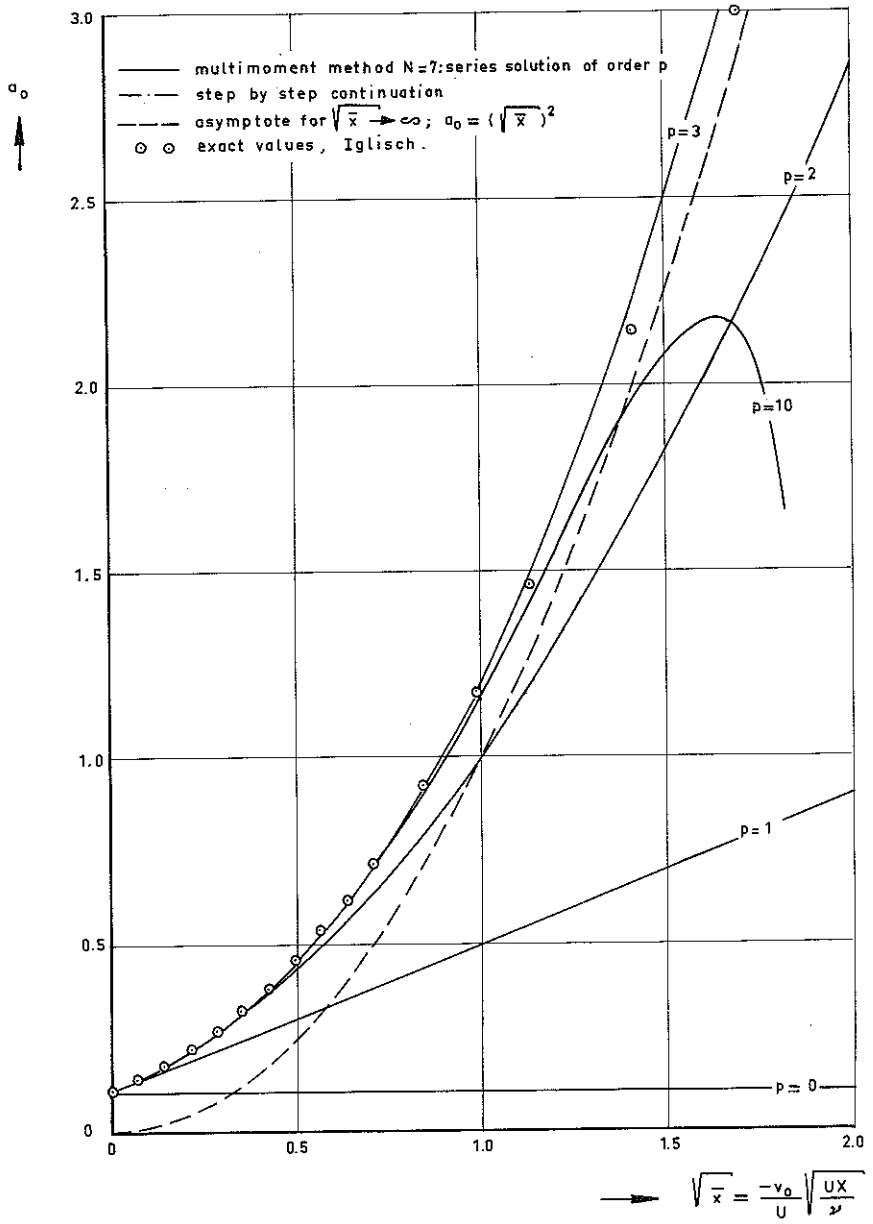

FIG. 8.25: SOME RESULTS OF THE MULTIMOMENT METHOD WITH N = 7 FOR THE FLAT PLATE WITH CONSTANT SUCTION VELOCITY.

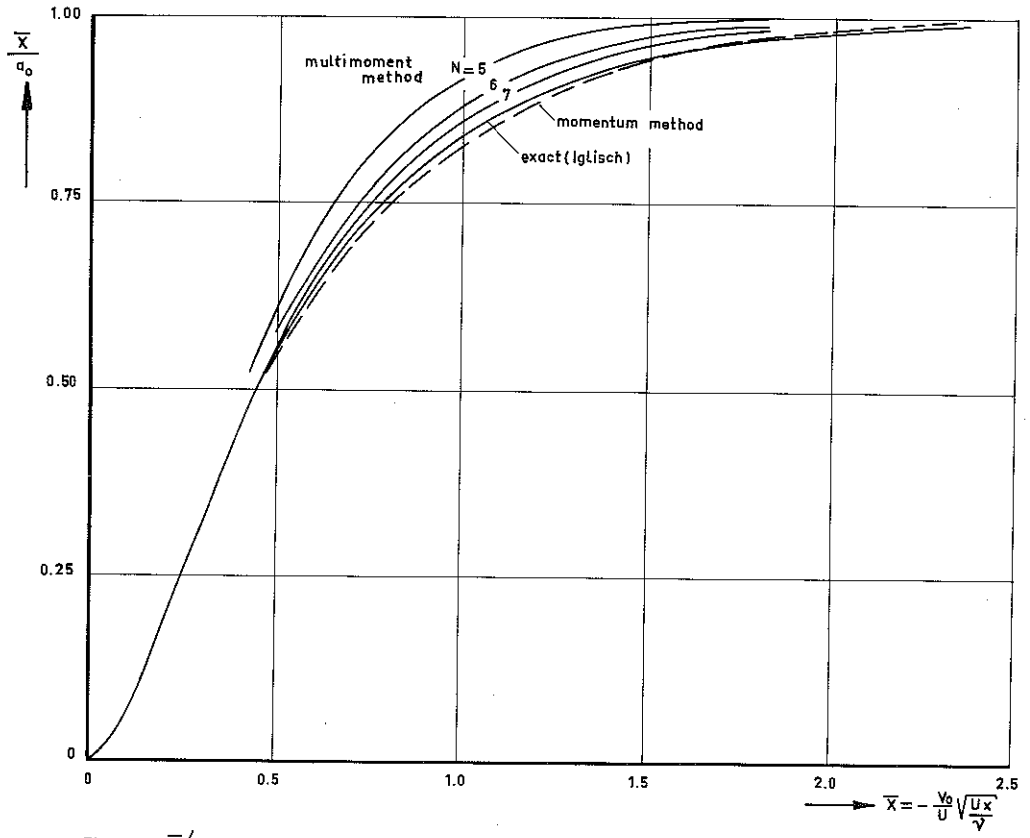

FIG. 8.26 : $\overline{X}/a_0$ FOR THE FLAT PLATE WITH CONSTANT SUCTION VELOCITY .

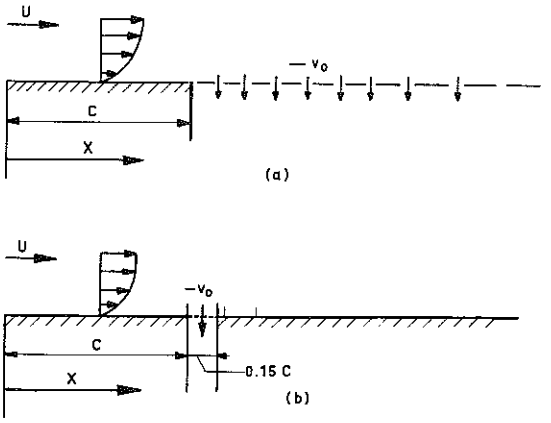

FIG. 8.27: TWO EXAMPLES OF BOUNDARY LAYERS WITH DISCONTINUOUSLY VARYING SUCTION VELOCITY DISCUSSED BY RHEINBOLDT .

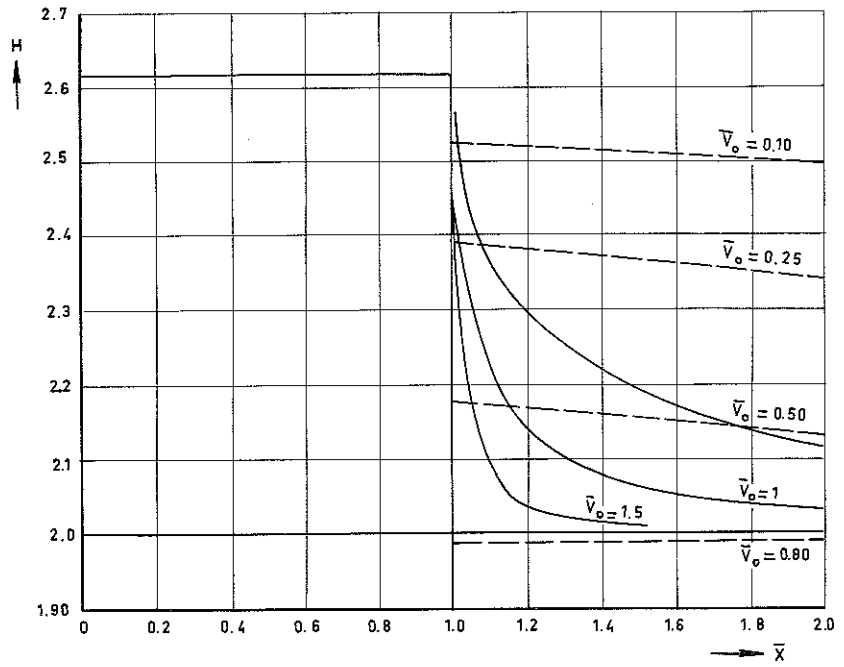

FIG. 8.28 : THE SHAPE FACTOR H FOR RHEINBOLDTS FIRST EXAMPLE ;
——— EXACT ; — — — MULTIMOMENT METHOD.

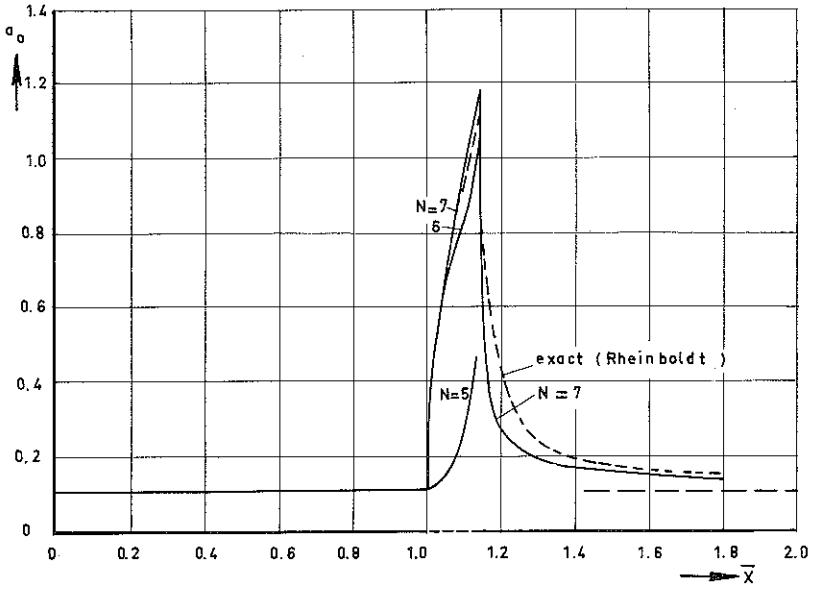

FIG. 8.29: RESULTS OF THE MULTIMOMENT METHOD FOR RHEINBOLDTS SECOND EXAMPLE.

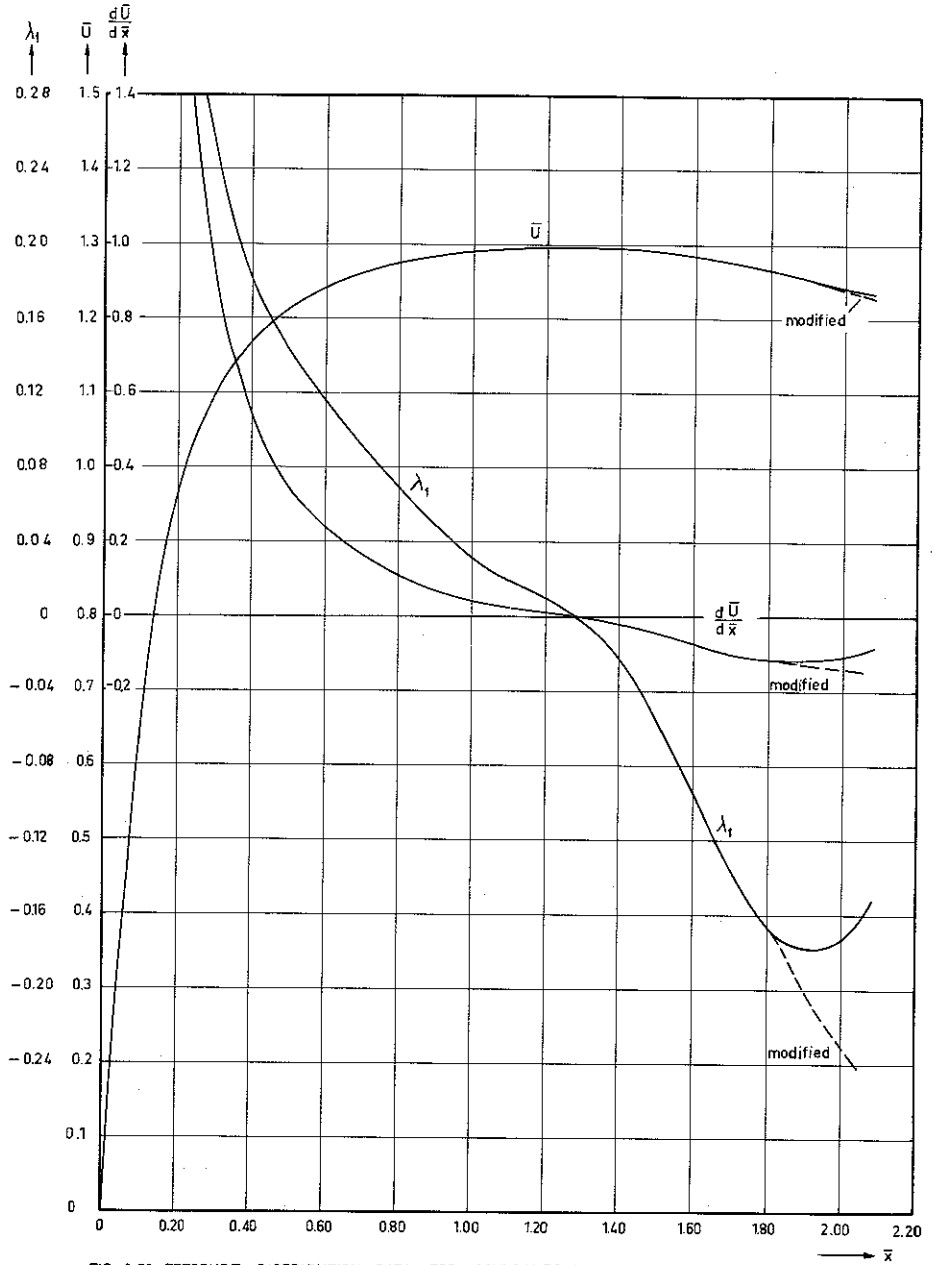

FIG. 8.30: PRESSURE DISTRIBUTION DATA FOR SCHUBAUER'S ELLIPS

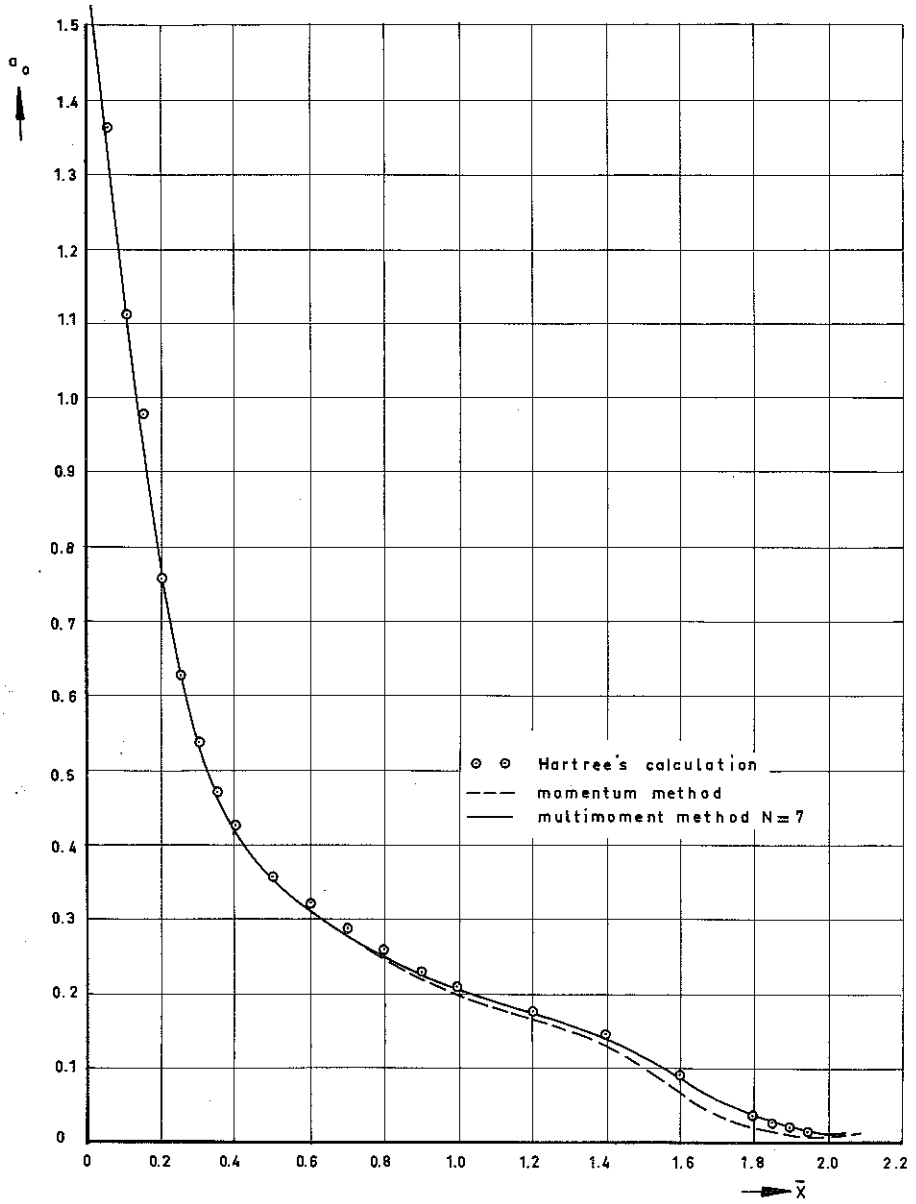

FIG. 8.31: THE WALL SHEAR STRESS PARAMETER a_0 FOR SCHUBAUER'S OBSERVED PRESSURE DISTRIBUTION.

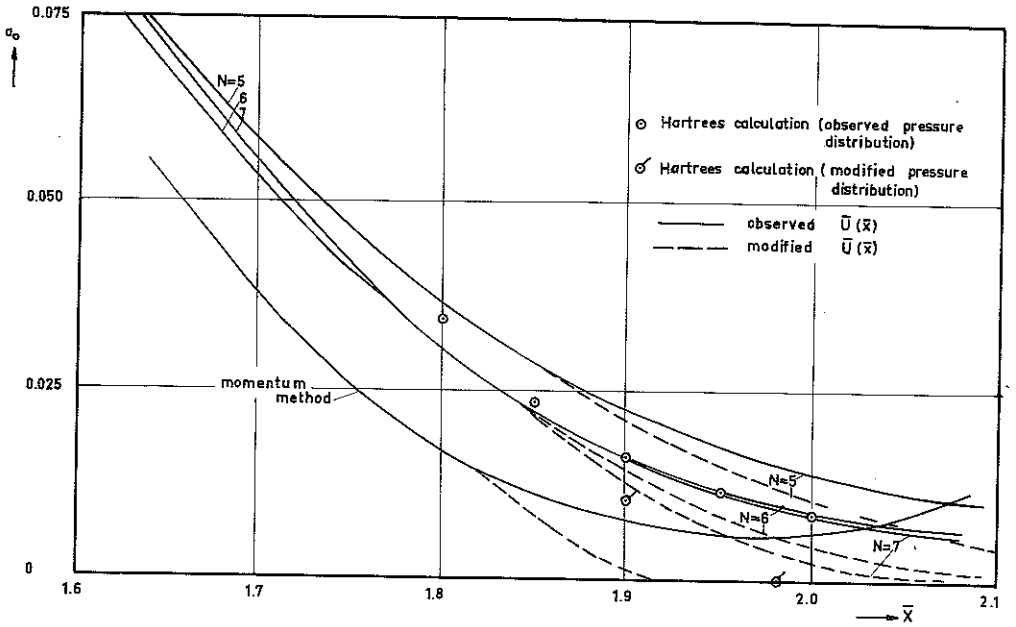

FIG. 8.32: THE SHEAR STRESS PARAMETER a_0 FOR SCHUBAUERS ELLIPTIC CYLINDER; OBSERVED AND MODIFIED PRESSURE DISTRIBUTION

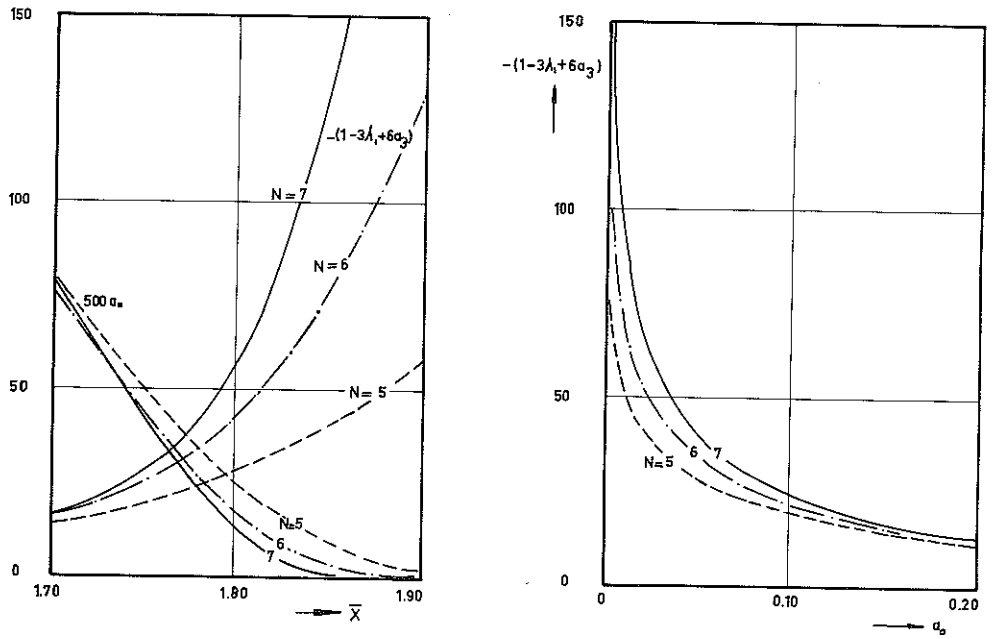

FIG. 8.33: BEHAVIOUR OF THE MULTIMOMENT METHOD NEAR SEPARATION FOR $\bar{U} = \sin\bar{x}$.